Chemical composition of Pluto aerosol analogues

Lora Jovanovic, Thomas Gautier, Véronique Vuitton, Cédric Wolters, Jérémy Bourgalais, Arnaud Buch, François-Régis Orthous-Daunay, Ludovic Vettier, Laurène Flandinet, Nathalie Carrasco

Chemical composition of Pluto aerosol analogues

Lora Jovanović[1], Thomas Gautier[1], Véronique Vuitton[2], Cédric Wolters[2], Jérémy Bourgalais[1], Arnaud Buch[3], François-Régis Orthous-Daunay[2], Ludovic Vettier[1], Laurène Flandinet[2], Nathalie Carrasco[1]

[1] LATMOS/IPSL, UVSQ - Université Paris-Saclay, Sorbonne Université, CNRS, Guyancourt, France

[2] Université Grenoble Alpes, CNRS, IPAG, Grenoble, France

[3] LGPM, CentraleSupélec, Université Paris-Saclay, Gif-sur-Yvette, France

Keywords

Pluto; Pluto, Atmosphere; Atmospheres, Chemistry; Organic chemistry

Abstract

Photochemical aerosols were observed in Pluto atmosphere during the *New Horizons* flyby on July 14th, 2015, as several thin haze layers extending at more than 350 km of altitude. This flyby has raised numerous questions on the aerosols formation processes and their impact on Pluto radiative transfer and climate. In order to gain a better understanding, we synthesized Pluto aerosol analogues in a room-temperature dusty plasma experiment and inferred their chemical composition from infrared spectroscopy, elemental composition analysis and very high-resolution mass spectrometry (ESI+/Orbitrap device). Three types of samples were synthesized at 0.9 ± 0.1 mbar, called P_{400}, P_{600} and $P_{CO\text{-}free}$. The samples P_{400} and P_{600} were produced from gas mixtures mimicking Pluto atmosphere at around 400 and 600 km of altitude, respectively, in order to determine if CH_4 mixing ratio has an influence on the chemical composition of the aerosols. The sample $P_{CO\text{-}free}$ was produced from a gas mixture similar to the one forming the sample P_{400}, but without carbon monoxide, in order to identify the impact of CO.

Our study shows that the molecules constituting samples P_{400} and P_{600} are very rich in nitrogen atoms (up to 45 % in mass of N elements) and, compared to the molecules constituting the $P_{CO\text{-}free}$ sample, a significant incorporation of oxygen atoms was detected. Moreover, our results on the variation of CH_4 mixing ratio demonstrate that different ratios lead to different reactivity between N_2, CH_4 and CO. In particular, more nitrogen and oxygen atoms are detected in the bulk composition of the analogues P_{400}. Due to the presence of nitrogenated and oxygenated molecules in the analogues of Pluto aerosols, we suggest that these aerosols will have an impact on Pluto radiative transfer, and thus on climate, that will differ from predictions based on the optical constants of Titan aerosol analogues.

I. Introduction

Since 1988, ground-based observations have shown that Pluto is surrounded by a tenuous atmosphere (Elliot et al., 1989; Hubbard et al., 1988), which is seasonal due to Pluto elliptic orbit. This atmosphere is supplied by the sublimation of the surface ices composed of molecular nitrogen N_2, methane CH_4 and carbon monoxide CO (Forget et al., 2017; Grundy et al., 2016; Owen et al., 1993; Stern et al., 2015). These observations motivated the establishment of the *New Horizons* mission, whose one of the goals was to characterize the structure, composition and variability of neutral atmosphere of Pluto (Young et al., 2008). The *New Horizons* spacecraft flew by Pluto at closest approach on July 14th, 2015, providing important information about Pluto atmosphere thanks to its suite of instruments.

From radio occultation data measured by the REX (Radio Experiment) instrument, the average surface pressure was measured at approximately 11 µbar, while the temperature near surface was estimated at about 45 K (Gladstone et al., 2016; Hinson et al., 2017). The composition of Pluto atmosphere was confirmed from solar ultraviolet occultation data recorded by the ALICE spectrograph (Young et al., 2018). Pluto atmosphere is mainly composed of N_2 – in vapor-pressure equilibrium with N_2 ice – and CH_4. In addition to these molecules, 515 ± 40 ppm of CO was detected with submillimeter observations by ALMA (Lellouch et al., 2017) and few hydrocarbons (C_xH_y) are also part of the atmosphere as trace species (Young et al., 2018).

Considering this atmospheric composition – a nitrogen-based atmosphere containing a substantial fraction of methane – and the presence of spikes in the lightcurve of the stellar occultation by Pluto on June 9th, 1988, the presence of photochemical aerosols was suspected and discussed since the 1990's (Elliot et al., 1989; Krasnopolsky and Cruikshank, 1999; Lara et al., 1997; Lellouch, 1994; Stansberry et al., 1989). These aerosols were finally evidenced when Pluto was investigated by *New Horizons*, by means of forward scattering observations and solar occultations. Pluto aerosols aggregate into several optically thin haze layers of about a few kilometers, extending at an altitude of > 350 km and accounting for about 0.1 ppm_V of the atmosphere (Cheng et al., 2017; Gladstone et al., 2016; Stern et al., 2015; Young et al., 2018). The blue color of the observed haze and the UV extinction exceeding unity are consistent with very small and forward-scattering particles (Rayleigh scatterers, with radius $r \sim 10$ nm), while the large forward scatter-to-back scatter ratio in the visible suggests much larger particles ($r > 0.1$ mm). Thus, the haze might be composed of randomly-shaped aggregates of spherical particles with different sizes (Cheng et al., 2017; Gladstone et al., 2016; Stern et al., 2015).

These aerosols may have a deep impact on Pluto atmospheric chemistry, for instance through the depletion from the atmosphere of small hydrocarbons that stick to the negatively-charged aerosols and may form complex hydrocarbons (Luspay-Kuti et al., 2017). They may also impact the climate of Pluto, such as playing the role of condensation nuclei for clouds (Lavvas et al., 2016; Luspay-Kuti et al., 2017). They can also influence the radiative cooling by absorbing 1 to 5 % of incident solar radiations, explaining why Pluto atmosphere, at about 400 km of altitude, is around 30 K colder than predicted by the models (Gladstone et al., 2016; Zhang et al., 2017; Zhu et al., 2014). Studying Pluto aerosols is thus of prime importance to understand the physics and the chemistry of Pluto atmosphere.

Recent photochemical models have been developed to explain the formation of aerosols in Pluto atmosphere, based on two processes (Cheng et al., 2017; Gladstone et al., 2016; Luspay-Kuti et al., 2017; Wong et al., 2017).
At lower altitudes, between 200 and 400 km, the condensation of volatiles onto photochemical aerosols dominates (Luspay-Kuti et al., 2017; Mandt et al., 2017; Wong et al., 2017). This condensation concerns C_2 hydrocarbons – C_2H_2, C_2H_4, C_2H_6 – HCN, CH_2NH, C_3H_4, C_3H_6, CH_3CN, C_4H_2, HC_3N, C_2H_3CN, C_2N_2, CH_3C_2CN and C_6H_6 (Gao et al., 2017; Krasnopolsky and Cruikshank, 1999; Lara et al., 1997; Luspay-Kuti et al., 2017; Mandt et al., 2017; Wong et al., 2017).

In the upper atmosphere, above 400 km of altitude, the aerosols formation is dominated by photochemistry (Gladstone et al., 2016; Wong et al., 2017; Young et al., 2018). By analogy with Titan, whose atmosphere is mainly composed of molecular nitrogen and methane, a complex photochemistry is initiated in Pluto upper atmosphere by far-ultraviolet sunlight and by solar photons that are scattered back to the Solar System by hydrogen present in interplanetary medium (Gladstone et al., 2016, 2015). This photochemistry involves neutral and ionic molecules generated from the ionization and the dissociation of N_2, CH_4 and CO, leading to the formation of complex hydrocarbons, nitriles and oxygenated organic molecules. Some of the molecules formed by photochemistry can then polymerize, resulting in the formation of aerosols. Nevertheless, the exact reactive pathways leading to the formation of Pluto photochemical aerosols are not well constrained yet.
In this study, we used the experimental setup PAMPRE developed at LATMOS (Guyancourt, France) to produce analogues of Pluto photochemical aerosols. This experimental device simulates the formation of aerosols by polymerization of molecules in the gas phase. The condensation of volatiles as occurring at low altitudes in Pluto atmosphere is therefore not reproduced in the simulation chamber, and is beyond the scope of this study.

Additionally, as Pluto aerosols are seen at least as high as 350 km of altitude, they are certainly formed higher in the atmosphere, but are there initially too small to scatter the photons in the UV-Visible range. Moreover, the data obtained by the ALICE spectrograph (Young et al., 2018) showed that the mixing ratio of CH_4 varies from 0.5 % at the surface to 50 % at about 1450 km of altitude. Due to this variability in atmospheric composition, it is legitimate to wonder about the variability in chemical composition of these aerosols.

The aim of this work is to constrain the chemical composition and the formation pathways of Pluto photochemical aerosols. We performed for this purpose very high-resolution mass spectrometry, infrared spectroscopy and elemental composition analyses of Pluto aerosol analogues.

II. Experimental setup and analyses protocol

1. PAMPRE

Pluto aerosol analogues were produced using the PAMPRE experimental setup, already described in detail in Szopa et al. (2006) and Alcouffe et al. (2010). PAMPRE is a Radio-Frequency Capacitively Coupled Plasma (RF CCP) generated in a gas mixture by a 13.56 MHz generator (*SAIREM GRP 01KE*). The interaction between the electrons from the discharge – mimicking the energy distribution of the solar photons (Szopa et al., 2006) – and the injected molecules produces a plasma in which the aerosol analogues are formed in volume. Before each experiment, the reactor is cleaned, heated and pumped down to a secondary vacuum of 1.5×10^{-6} mbar. The gas mixture is introduced in the stainless-steel reactor through the meshed polarized electrode, as a homogeneous and continuous flow, and is extracted by a primary vane pump (*Adixen by Pfeiffer Vaccuum Pascal 2015 SD*). In this work, the gas mixture introduced in the reactor, expected to be representative of Pluto atmosphere, is composed of molecular nitrogen N_2 and methane CH_4 – in variable proportions – and 500 ppm of carbon monoxide CO (*Air Liquide*, with impurities H_2O < 3 ppm, O_2 < 2 ppm and C_xH_y < 0.5 ppm).

For the experiments presented here, the total flow rate was set at 55 sccm (standard cubic centimeters per minute), controlled by gas flow controllers (*MKS*), resulting in an overall plasma pressure of 0.9 ± 0.1 mbar, at ambient temperature. Note that the pressure and temperature are higher in the experiment than in Pluto upper atmosphere (~ 10^{-2} µbar and ~ 65 K at 400 km of altitude and ~ 10^{-4} µbar and ~ 65 K at 600 km of altitude (Gladstone and Young, 2019)). However, the most important parameter, the ionization rate, is the same and in the order of ppm_v. As ion-molecule reaction rates are relatively insensitive to low temperatures (Anicich et al., 2003; Böhme, 2000; Imanaka and Smith, 2009), the lower temperature in Pluto upper atmosphere (65 K instead of 293 K in our experiment) is not an issue in our case. The higher pressure induces shorter mean free path for the molecules, which main implication is just faster kinetics in the experiment. This remains true as long as the pressure is low enough to minimize trimolecular reactions (a few mbar), which is the case in all our experiments. In contrast, using similar ionization rate enables a realistic contribution of ions into the whole ion-neutral coupled chemical network and thus better represents Pluto atmospheric chemistry.

The plasma is confined in a cylindrical metallic cage where the particles form. The cage contains grid apertures allowing the aerosol analogues to be ejected out of the plasma and to accumulate as a brownish powder on glass vessel walls surrounding the confining cage. The aerosol analogues were finally collected at atmospheric pressure for the *ex situ* analyses presented below.

2. Sample synthesis: Pluto aerosol analogues

In this work, two types of Pluto aerosol analogues were synthesized. The first one was produced from a gaseous mixture containing 99 % of N_2, 1 % of CH_4 and 500 ppm of CO, representative of the aerosols forming at 400 km of altitude in Pluto atmosphere – we will thereafter call it P_{400}. The second type was produced from a gaseous mixture containing 95 % of N_2, 5 % of CH_4 and 500 ppm of CO, which is representative of aerosols that could form at 600 km of altitude – thereafter called P_{600} (Lellouch et al., 2017; Young et al., 2018).

In order to understand the impact of the presence of CO in Pluto atmosphere, aerosol analogues were also synthesized from a plasma containing 99 % of N_2 and 1 % of CH_4, but without CO. This type of analogue, afterward called $P_{CO\text{-}free}$ – equivalent to Titan aerosol analogues– has been studied for decades (Cable et al., 2012; Coll et al., 2013, 1999; Imanaka et al., 2004; Imanaka and Smith, 2010; Khare et al., 1984; McDonald et al., 1994; Sciamma-O'Brien et al., 2017; Sekine et al., 2008; Szopa et al., 2006) (Table 1).

Table 1: Table presenting the three samples analyzed in this study.

Composition of the reactive mixture			Corresponding altitude on Pluto	Acronym of the aerosol analogues
N_2	CH_4	CO		
99 %	1 %	500 ppm	400 km	P_{400}
95 %	5 %	500 ppm	600 km	P_{600}
99 %	1 %	-	-	$P_{CO\text{-}free}$

3. Infrared spectroscopy by the Attenuated Total Reflectance technique

The infrared spectra of Pluto aerosol analogues were acquired using an Attenuated Total Reflectance (ATR) accessory on the *Thermo Scientific Nicolet 6700* spectrometer, driven by *OMNIC* software. The purpose of this analysis was to characterize the chemical functions present in the molecules constituting the samples.

A spatula tip of the aerosol analogues was deposited on a zinc selenide (ZnSe) crystal. Direct contact between the sample and the crystal was facilitated by applying pressure to the sample. An IR beam was directed onto the crystal at an angle of incidence greater than a critical angle. Under these conditions, an evanescent wave was generated and passed through the sample for a few micrometers (0.5 to 5 µm). Depending on the chemical functions present in the molecules constituting the aerosol analogues, the evanescent wave is absorbed at different characteristic wavelengths. The resulting altered wave was collected by a DTGS KBr (deuterated-triglycine sulfate, potassium bromide) detector.

The spectrum presented here results from the accumulation of 250 scans, acquired between 500 and 4000 cm^{-1}, with a resolution of 4 cm^{-1} corresponding to a digital increment of 1.928 cm^{-1}. Background spectrum was also acquired before the sample analysis, to remove the contribution of ambient atmosphere.

4. Sample preparation for very high-resolution mass spectrometry analysis

To analyze the molecular composition of the aerosol analogues by very high-resolution mass spectrometry (ESI+/Orbitrap technique), we dissolved about 1 mg of the samples in 1 mL of a 50/50 % (v/v) methanol/acetonitrile (*Carlo Erba*, UHPLC-MS quality) mixture (MeOH/ACN) in a polypropylene vial at ambient conditions. The choice of the solvent was based on Titan aerosol analogues literature, extracting most of the soluble fraction (Carrasco et al., 2009; Somogyi et al., 2005). The vials were then agitated and centrifuged for few minutes and then, the supernatants were diluted at 0.5 mg/mL in order to stabilize the ionization source and to optimize the ionization yield.

5. Very High-Resolution Mass Spectrometry by the ESI+/Orbitrap technique

In order to determine the stoichiometric formulae of the molecules constituting the soluble fraction of Pluto aerosol analogues, we analyzed them by Very High-Resolution Mass Spectrometry (VHRMS). We used the analytical instrument *LTQ Orbitrap™ XL* (*ThermoFisher Scientific*) installed at IPAG (Grenoble, France), a Fourier Transform mass spectrometer combining two mass analyzers: a Linear Trap Quadrupole (LTQ) and an Orbitrap (Makarov et al., 2006; Perry et al., 2008). The LTQ selects the ions belonging to a specific mass range and brings them to the C-trap. The C-trap then accumulates the ions and focalizes them to the Orbitrap, which acts as mass analyzer. The ionization source was the ElectroSpray Ionization (ESI) in positive mode (ESI+) (Banks and Whitehouse, 1996; Yamashita and Fenn, 1984). ESI+ is a "soft" ionization method producing mainly mono-charged (and few multi-charged) ions by adding protons (H^+) without any substantial fragmentation of the molecules. This positive mode of ionization has been widely used for Titan aerosol analogues analysis in the literature (Sarker et al., 2003; Somogyi et al., 2016, 2012, 2005; Vuitton et al., 2010) and, as a "soft" ionization method, gives access to the pristine molecules present in the soluble fractions of interest. Furthermore, elemental composition analysis of Titan aerosol analogues produced with different proportions of CO has shown that nitrogen and oxygen atoms are substantial components of the samples (Fleury et al., 2014). The ESI+ source is thus adapted to the analysis of our samples due to the proton affinity of the nitrogen and oxygen atoms constituting our analyzed molecules (Rodgers et al., 2005). Nevertheless, it should be kept in mind that this technique can only study the soluble fraction of the samples, which probably represents only 20 to 35 % of the total solid mass of Pluto aerosol analogues (Carrasco et al., 2009).

The sample was injected into the ESI+ source using a syringe through a polyetheretherketone (PEEK) capillary (direct infusion) with a fixed flow of 3 µL/min. The capillaries were systematically washed with methanol between each sample analysis. The analyses were performed using *Thermo Tune Plus* software, with the following ESI+ source parameters: a spray voltage of 3.5 kV, a sheath gas flow rate of 5 (arbitrary unit), an aux gas flow rate of 0 (arbitrary unit), a sweep gas flow rate of 0 (arbitrary unit), a capillary voltage of 34 V, a capillary temperature of 275 °C and a tube lens voltage of 50 V.

As we estimated that no unequivocal molecular assignment can be made above *m/z* 300 due to the high complexity of the material analyzed (Gautier et al., 2014), we restricted our analysis from *m/z* 50 to *m/z* 300.

In order to increase the signal/noise ratio, each mass spectrum is the mean of 4 scans and each scan is the sum of 128 microscans. The maximum ion injection time allowed into the Orbitrap was 500 ms. The mass spectra were acquired with a resolution $m/\Delta m$ set to 100,000 at *m/z* 400.

6. Calibration of the VHRMS data and identification of the molecules

Prior to the analyses, the Orbitrap was externally calibrated with a mixture of caffeine, MRFA peptide and Ultramark. No internal calibration was used. Mass spectra of blanks (solvent only) were also acquired before each analysis of the samples $P_{CO\text{-}free}$, P_{400} and P_{600}. Molecules present in the blanks were subsequently removed from the samples analyses (see an example of blank

mass spectrum in Supplementary Material, Figure A). The external calibration was not sufficient on a small *m/z* scale, because the lightest calibrator, the caffeine, was at *m/z* 195. Thus, *Attributor*, a software developed at IPAG (Grenoble, France) (Orthous-Daunay et al., 2019), was also used to improve the calibration of the data. We used the masses of molecules known to be present in the $P_{CO\text{-}free}$ sample (Gautier et al., 2014) to refine the calibration curve to correct the mass spectra of Pluto aerosol analogues: $C_3N_2H_5^+$ at *m/z* 69.045 and $C_4N_2H_7^+$ at *m/z* 83.060.

Attributor was also used to attribute the stoichiometric formulae to the molecules constituting the samples. For the molecules assignment, we excluded the peaks whose intensity was four orders of magnitude lower than the most intense peak. The attribution was based on a combination of *x* carbon, *y* hydrogen, *z* nitrogen and *w* oxygen ($C_xH_yN_zO_w$). The considered isotopes were: ^{12}C, ^{1}H, ^{14}N and ^{16}O. To avoid aberrant formulae, we used some restrictions. The minimum numbers of carbon, hydrogen and nitrogen atoms were set to 1 and there were no maximum numbers. The minimum number of oxygen atom was set to 0 and the maximum number limited to 3; due to the low proportion of CO injected in the reactor, it is unlikely to form highly-oxygenated molecules. Theoretical *m/z* with a deviation more than ± 5 ppm were excluded (according to the instrument specifications in external calibration mode). An additional filter was applied to screen out unrealistic molecules with H/C > 5 and N/C > 3 ratios, which would be molecules with extremely exotic structures and/or C atoms with more than four bonds.

7. Elemental composition analysis

An elemental composition analysis of P_{400} and P_{600} samples was performed to determine their carbon, hydrogen, nitrogen and oxygen mass percentages.

The determination of C, H and N was performed using a Flash*Smart*™ elemental analyzer (*ThermoFisher Scientific*) under flash combustion at 930 °C. About 1-2 mg of each sample, with 1 mg of vanadium pentoxide (V_2O_5) for complete combustion, were precisely weighed into a tin container. For the determination of O, the system operated in pyrolysis mode at 1050 °C. About 1-2 mg of each sample were weighed into a silver container. Then, tin and silver capsules were individually introduced into the combustion reactor via the *Thermo Scientific™ MAS Plus Autosampler*. After combustion (C, H and N) and pyrolysis (O), the resulting gases – CO_2, H_2O and N_2 – were transported by a helium flow to a copper-filled layer and then swept through a gas chromatography (GC) column to separate the combustion gases. Finally, they were detected by a Thermal Conductivity Detector (TCD).

Two calibration curves have been created: one for C, H and N measurements and one for O measurements. For this purpose, 0.5-5 mg of BBOT (2,5-Bis(5-ter-butyl-benzoxazol-2-yl) thiophene**,** $C_{26}H_{26}N_2O_2S$) (*Fisher Scientific*, 99 % purity) were analyzed as a standard using K factor as the calibration method.

III. Results

1. ESI+/Orbitrap analysis

Figure 1 presents the ESI+/Orbitrap mass spectrum of the soluble fraction of Pluto aerosol analogues P_{400}, from *m/z* 50 to *m/z* 300. Intensity was normalized to the most intense peak in the mass spectrum (*m/z* 127.0725).

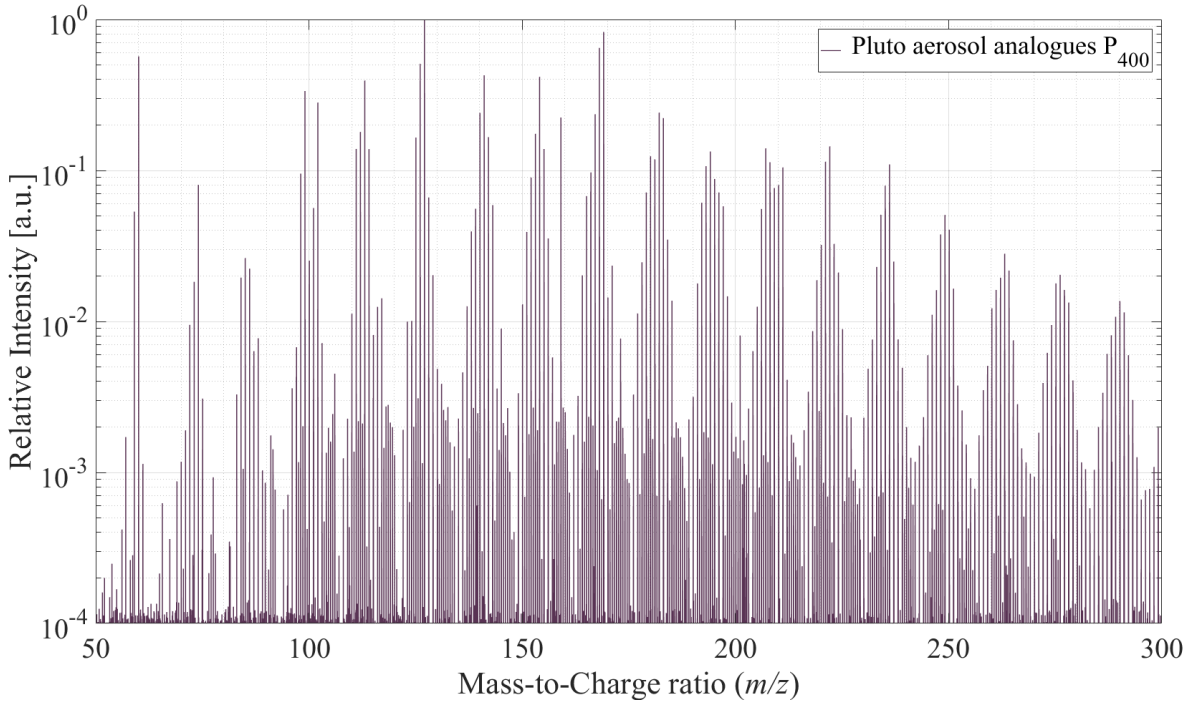

Figure 1: ESI+/Orbitrap mass spectrum of the soluble fraction of Pluto aerosol analogues P_{400}. The *x*-axis corresponds to the Mass-to-Charge ratio (*m/z*), while the *y*-axis corresponds to the relative intensity of the peaks, normalized to the most intense peak (*m/z* 127.0725). The small peaks in dark purple color are due to an aliasing effect.

In the mass spectrum (Figure 1), thousands of peaks are seen; hence, the soluble fraction of Pluto aerosol analogues is a complex mixture requiring such a high-resolution and high-precision analysis. The peaks are grouped in several periodic clusters similar to those observed in the mass spectrum of Titan aerosol analogues. This analogy suggests that the molecules detected in the soluble fraction of Pluto aerosol analogues, using ESI+/Orbitrap, are of a random-copolymeric nature, composed at least partially of a repetition of a $(CH_2)_m(HCN)_n$ pattern (Gautier et al., 2017; Maillard et al., 2018; Pernot et al., 2010).

2. Chemistry with N_2 and CO

From laboratory studies of Titan atmosphere we have learnt that not only methane, but also nitrogen plays a critical role in the atmospheric chemistry of Titan and in the formation and the growth of the aerosols (Carrasco et al., 2012; Dubois et al., 2019; Gautier et al., 2011; He and Smith, 2014, 2013; Hörst et al., 2018; Imanaka et al., 2004; Imanaka and Smith, 2010; Trainer et al., 2012). Our results emphasize the importance of nitrogen chemistry on Pluto as well.

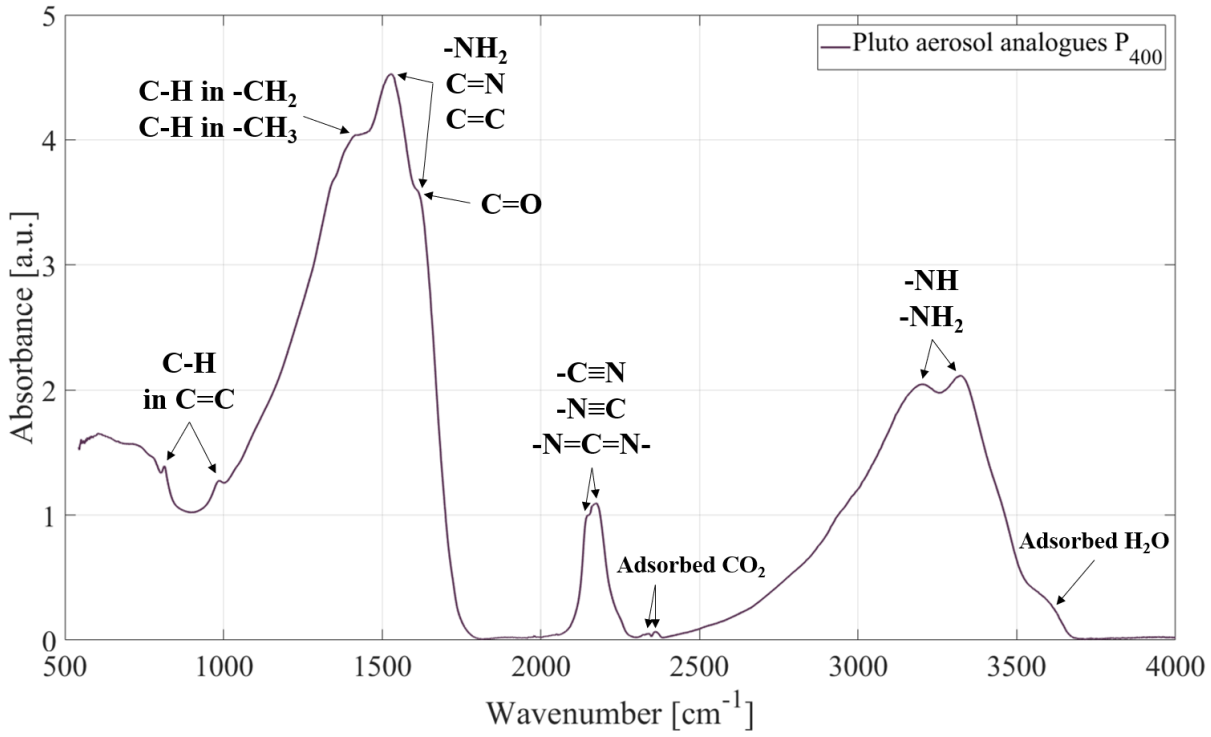

Figure 2: Infrared spectrum of Pluto aerosol analogues P_{400}, acquired by the ATR technique. At 2340 and 2360 cm^{-1}, small absorption bands are attributed to CO_2 adsorbed on the sample, while the shoulder at 3600 cm^{-1} corresponds to water adsorbed on the analogues as hydroxyl –OH.

Figure 2 presents the infrared spectrum of Pluto aerosol analogues P_{400}, obtained by the ATR technique. In this spectrum, the importance of N-bearing chemical functions is clearly shown (Gautier et al., 2012). At 1550 cm^{-1}, a strong absorption band can be attributed to the deformation vibrations of aromatic and aliphatic amines $–NH_2$ and of double bonds C=C and C=N in aromatic and hetero-aromatic cycles. The bands at 2150 and 2170 cm^{-1} can be attributed to nitriles –C≡N, isocyanides –N≡C and carbodiimides –N=C=N–. At 3200 and 3330 cm^{-1}, there are two strong large bands, characteristic of primary and secondary amines –NH and $–NH_2$.

According to the IR spectrum (Figure 2) and due to the selectivity of the ESI+ source (Rodgers et al., 2005), we expect to detect with the Orbitrap a large amount of N-bearing organic molecules in the soluble fraction of P_{400} and P_{600} samples. The presence of oxygenated organic molecules is also expected. In contrast, we do not expect to detect hydrocarbons without heteroatoms, since this kind of molecules is minor in similar samples (Derenne et al., 2012; Gautier et al., 2016, 2014; Morisson et al., 2016). In addition, the ESI+ source is not the most adequate to detect them due to their low proton affinity (Molnárné Guricza and Schrader, 2015).

In order to understand if the presence of CO in Pluto atmosphere has an impact on the molecular composition of Pluto aerosols via the presence of oxygenated organic molecules, we compared the intensities of the oxygenated molecules present in the soluble fraction of Pluto aerosol analogues P_{400} and of aerosol analogues produced without CO (Figure 3). The intensities of the oxygenated molecules were normalized to the intensity of the most intense peak in the mass spectrum (*m/z* 127.0725 for P_{400} sample and *m/z* 60.0551 for $P_{CO\text{-}free}$ sample, respectively).

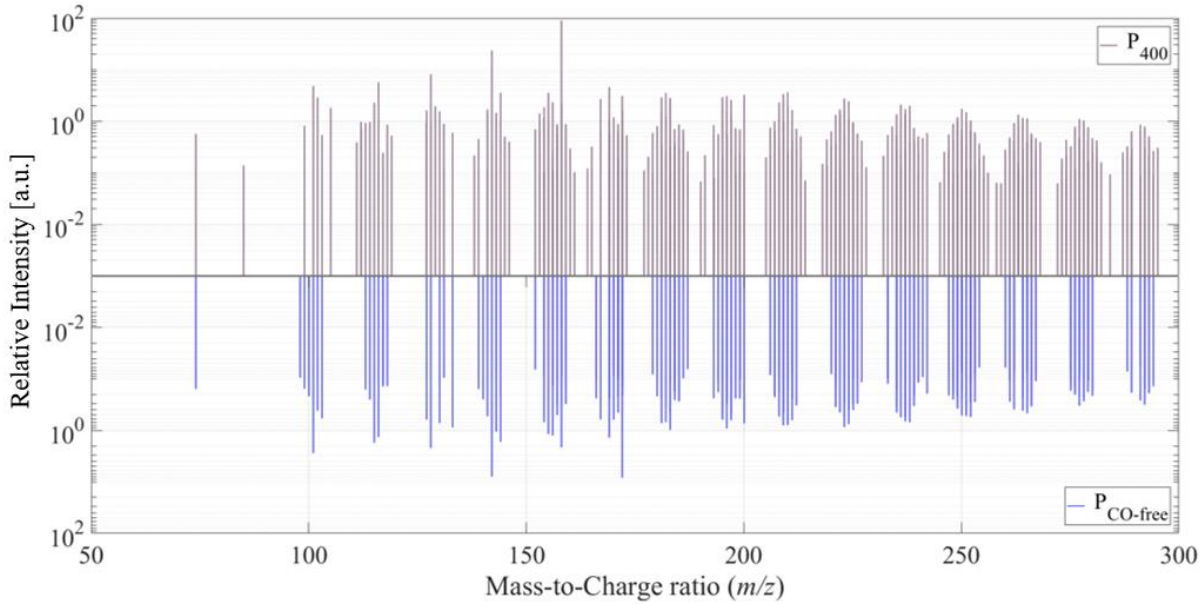

Figure 3: Normalized intensities of only the oxygenated molecules present in the soluble fraction of Pluto aerosol analogues P_{400} (in purple) and of aerosol analogues produced without CO ($P_{CO\text{-}free}$, in blue). The spectra were acquired with the ESI+/Orbitrap technique. Intensities were normalized to the most intense peak of each mass spectrum (*m/z* 127.0725 for P_{400} sample and *m/z* 60.0551 for $P_{CO\text{-}free}$ sample, respectively).

Upper panel in Figure 3 displays in purple the normalized intensities of oxygenated molecules present in the soluble fraction of Pluto aerosol analogues P_{400}. Lower panel (in mirror) shows in blue the normalized intensities of oxygenated molecules present in the soluble fraction of hypothetical Pluto aerosol analogues $P_{CO\text{-}free}$.

Considering the composition of the gas mixture producing the aerosol analogues without CO, oxygenated molecules should not be present. However, in this case, the small proportion of oxygenated molecules are produced by partial oxidation of the surface of the particles during the air exposure when collecting the samples (Carrasco et al., 2016; Fleury et al., 2014).

In Figure 3, the oxygenated molecules detected with ESI+/Orbitrap in Pluto aerosol analogues P_{400} appear to be similar to the oxygenated molecules contaminating the aerosol analogues without CO ($P_{CO\text{-}free}$). However, regarding the normalized intensities of these oxygenated molecules, it appears that they are significantly higher in P_{400} analogues than in $P_{CO\text{-}free}$, demonstrating an effective reactivity of CO.

The oxygenated molecules are detected at the same *m/z* ratios, within the accuracy of the Orbitrap, so that the chemical formulae attributions are the same. This means that the reactive pathways leading to their formation for P_{400} in the experiment might be, at least partially, similar to the oxidation pathways affecting $P_{CO\text{-}free}$. The oxygenated molecules present in P_{400} are produced both by reactions within the plasma simulating Pluto atmospheric chemistry and by surface oxidation of the particles during the collecting exposed to air. Both processes might involve the same oxidizing agents.

Future experiments would provide information on the oxidizing agents involved in the plasma oxidation pathways: analysis of the gas phase chemical composition of the plasma simulating Pluto atmosphere and synthesis of Pluto aerosol analogues with $C^{18}O$.

Figure 4 shows the molecules present in P_{400} (in purple) and $P_{CO\text{-}free}$ (in blue) samples, between *m/z* 492.20 and *m/z* 493.32 (arbitrary zooming for example purpose). The purple stars point out molecules that are present only in the sample P_{400}. Although the resolution of the analytical instrument is not sufficient above *m/z* 300 to strictly identify molecules, Figure 4 demonstrates that CO reactivity impacts the aerosols composition even at large masses.

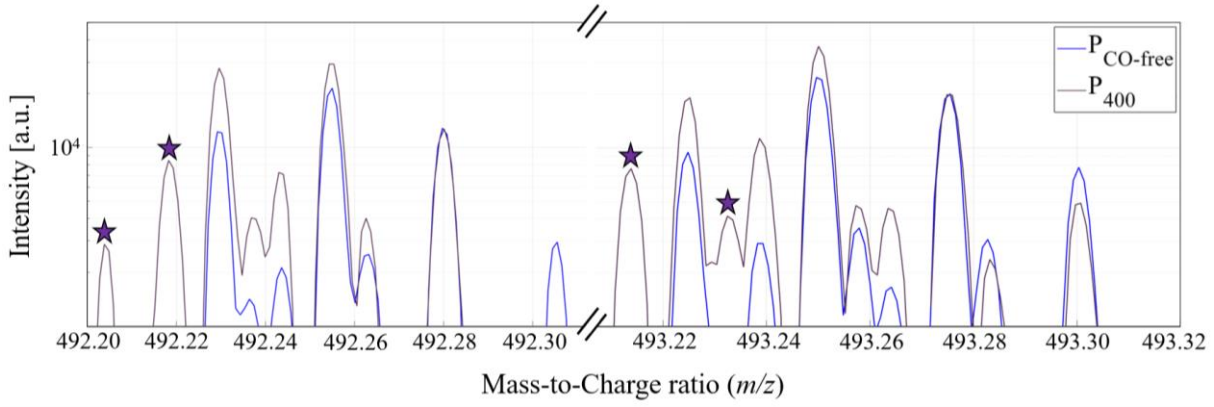

Figure 4: Mass spectra of P_{400} (in purple) and $P_{CO\text{-}free}$ (in blue) samples, between *m/z* 492.20 and *m/z* 493.32. The *x*-axis was cropped (//) for a better visualization of the peaks. The purple stars correspond to molecules that are detected only in the analogues P_{400}.

In Figure 4, we count 19 peaks. Of these, 14 stoichiometric formulae are common to both P_{400} and $P_{CO\text{-}free}$ samples, 1 formula is present only in the sample $P_{CO\text{-}free}$, while 4 formulae – those pointed out by the purple stars – are present only in the sample P_{400}. We can therefore conclude that the presence of CO in the reactive mixture, even in a small proportion (500 ppm), has an impact on the chemistry leading to the formation of aerosols on Pluto, from light gas-phase molecules to large macromolecular polymeric structures incorporated in the aerosols.

3. Effect of the altitude of aerosols formation

The mixing ratio of CH_4 in Pluto atmosphere strongly varies with the altitude (Young et al., 2018). This variation can have an impact on the molecular composition and thus on physical properties of Pluto aerosols.

As the abundance of CO is nearly constant all along Pluto atmosphere, the CO/CH_4 ratio varies with the variation of CH_4 mixing ratio, from 0.1 at the surface to 0.001 at around 1450 km of altitude. We therefore also study the distribution of the oxygenated molecules in Pluto aerosol analogues P_{600}.

In Figure 5, we compare the normalized intensities of the oxygenated molecules detected with ESI+/Orbitrap in the soluble fraction of P_{400} (upper panel, in purple) and P_{600} (lower panel, in mirror, in red). The intensities of the oxygenated molecules were normalized to the intensity of the most intense peak in the mass spectrum (*m/z* 127.0725 for P_{400} sample and *m/z* 60.0551 for P_{600} sample, respectively).

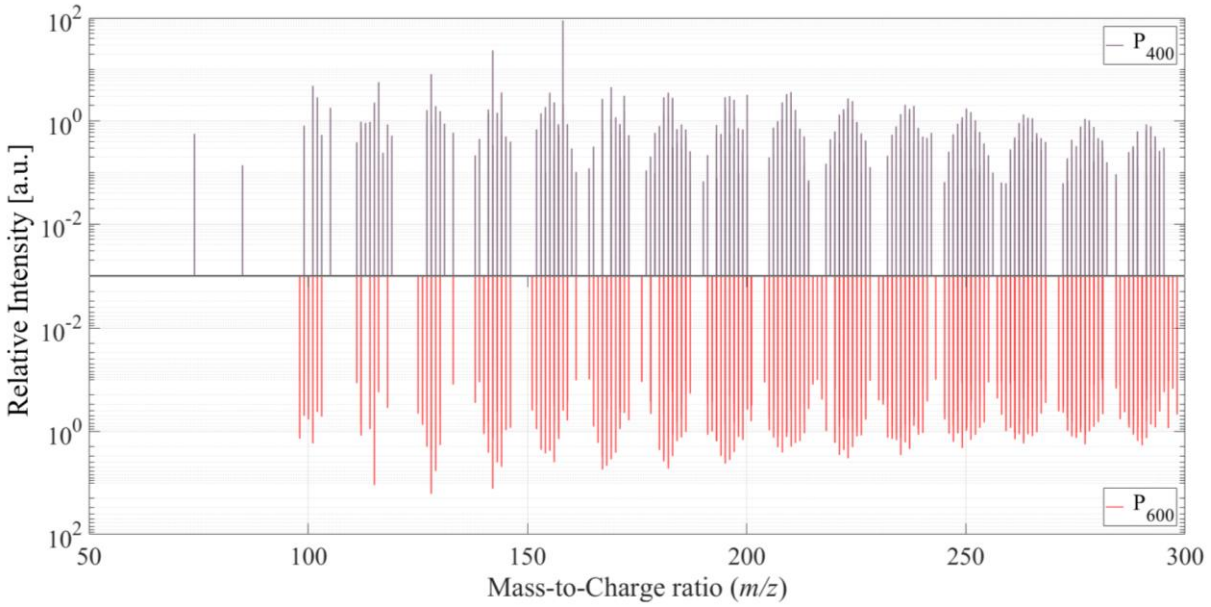

Figure 5: Normalized intensities of only the oxygenated molecules present in the soluble fraction of Pluto aerosol analogues P_{400} (in purple) and P_{600} (in red). The spectra were acquired with the ESI+/Orbitrap technique. The intensities of the peaks identified as oxygenated molecules have been normalized to the most intense peak of each mass spectrum (*m/z* 127.0725 for P_{400} sample and *m/z* 60.0551 for P_{600} sample, respectively).

Regarding the mass spectra on Figure 5, it seems that the clusters in P_{600} are shifted leftward compared to P_{400}, suggesting that the oxygenated molecules in the soluble fraction of P_{600} are different from those constituting the soluble fraction of P_{400}. This would imply that the chemical pathways leading to the formation of oxygenated molecules are quite different in Pluto aerosols depending on their altitude of formation. Due to the leftward shifting of the clusters, we can suppose that the oxygenated organic molecules detected in the soluble fraction of the sample P_{600} include less hydrogen atoms than the molecules present in the soluble fraction of P_{400}. Oxygenated organic molecules in P_{600} are therefore more unsaturated. From this observation, we can conclude that the increase in the mixing ratio of CH_4 (thus being at higher altitude on Pluto) leads to an increased formation of unsaturated molecules in the soluble fraction of Pluto aerosol analogues. This conclusion was also made for Titan aerosol analogues produced from N_2:CH_4 gas mixtures with different CH_4 mixing ratios (Derenne et al., 2012; Gautier et al., 2014). This implies that this effect is likely due to the variation in the mixing ratio of CH_4 itself and not to the presence of CO in the reactive mixture.

In order to determine the abundances of C, H, N and O atoms in Pluto aerosol analogues, we performed an elemental composition analysis of P_{400} and P_{600} samples and obtained the results presented in Table 2.

Table 2: Mass percentages of C, H, N and O elements present in Pluto aerosol analogues P_{400} and P_{600}. Given uncertainties correspond to ± 3σ.

Mass percentage (%)	P_{400}	P_{600}
C	42.1 ± 0.2	49.0 ± 0.2
H	3.7 ± 0.06	4.8 ± 0.07
N	45.1 ± 0.2	36.0 ± 0.2
O	1.9 ± 0.03	1.7 ± 0.03

Table 2 displays the mass percentages of the elements C, H, N and O present in Pluto aerosol analogues P_{400} and P_{600}. Note for both samples that the sum of the mass percentages does not equal 100 %. This is due to uncertainties related to the fact that the measurement of the mass percentage of the element O is not carried out at the same time, nor with the same technique, as the measurement of the mass percentages of the elements C, H and N.

Two observations can be deduced from Table 2: (1) sample P_{600} contains more carbon and hydrogen in mass, but less nitrogen than sample P_{400}; (2) sample P_{400} contains more oxygen in mass than sample P_{600}. The first observation can be explained by the fact that the sample P_{600} is synthesized with a higher CH_4 mixing ratio; whereby more C and H atoms and less N atoms are present in the reactive mixture. The second one, in agreement with the conclusion of He et al. (2017), is due to the fact that the sample P_{400} is produced with a higher CO/CH_4 ratio.

To further visualize the chemical differences between the soluble fraction of the samples P_{400} and P_{600}, we modified conventional van Krevelen [H/C versus O/C] diagrams. The van Krevelen diagrams were proposed in 1950 to study the structure and reactions processes of coal. Since then, this type of representation has been frequently applied on data obtained with high-resolution mass spectrometry (Kim et al., 2003; Marshall and Rodgers, 2008; Rodgers et al., 2005; Wu et al., 2004). More recently, this tool was expanded to the analysis of complex organic mixtures of terrestrial and planetary interests, using [H/C versus N/C] axes (Danger et al., 2016; Gautier et al., 2014; Imanaka and Smith, 2010; Pernot et al., 2010; Somogyi et al., 2012; Tziotis et al., 2011).

Figure 6 shows the modified van Krevelen diagrams of all the molecules identified in the soluble fraction of the samples P_{400} (top), P_{600} (middle) and $P_{CO\text{-}free}$ (bottom). The *x*-axis corresponds to Nitrogen-to-Carbon (N/C) ratio and the *y*-axis corresponds to Hydrogen-to-Carbon (H/C) ratio. Each point represents a given molecule constituting the soluble fraction of the sample analyzed by ESI+/Orbitrap. The colors correspond to the number of oxygen atoms included in the molecule. As the oxygen is not supposed to take part to the co-polymeric growth, due to its bivalence and its affinity to labile hydrogen (Decker and Jenkins, 1985; Ligon et al., 2014), but instead to be randomly included in the molecules, we have chosen to represent the data with the number of oxygen atoms present in the molecules and not with Oxygen-to-Carbon (O/C) ratio.

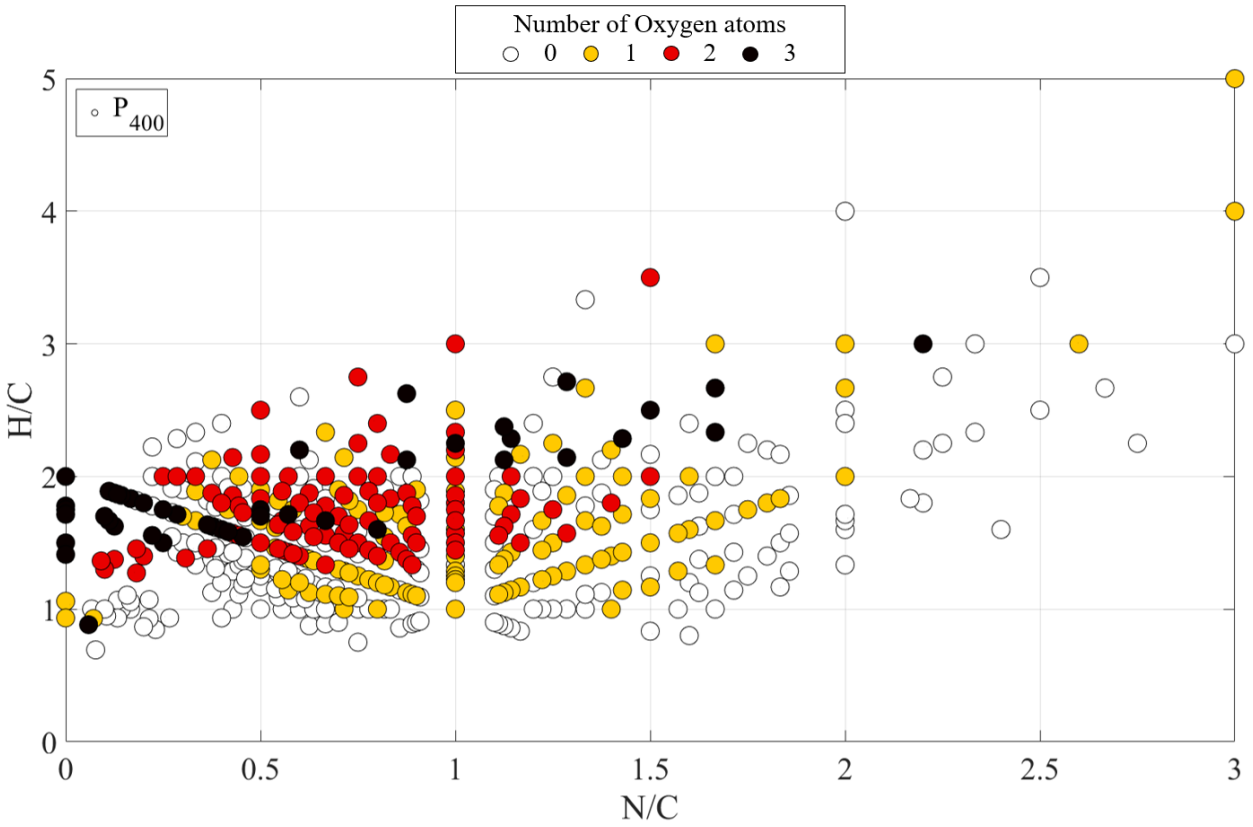
Number of Oxygen atoms
0 1 2 3
P400
H/C
N/C
0
0.5
1
1.5
2
2.5
3
0
1
2
3
4
5

436

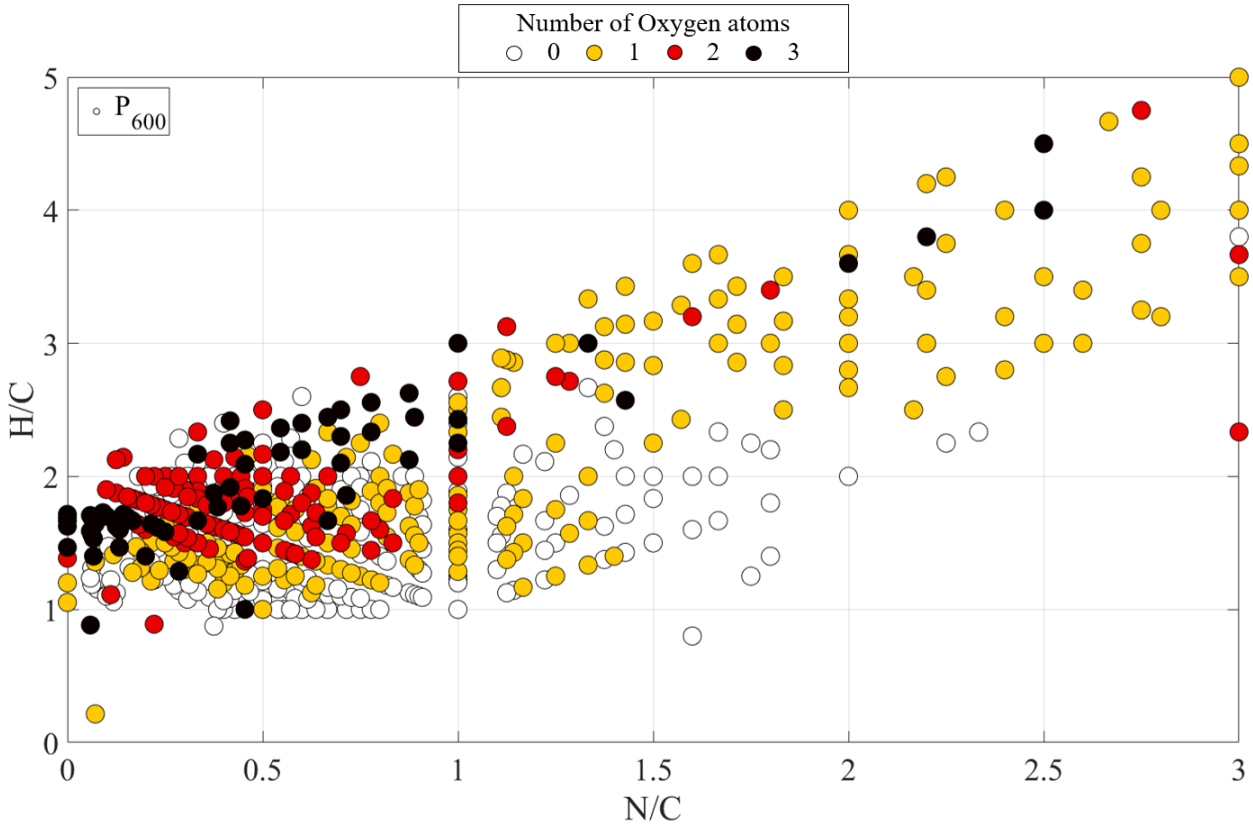
Number of Oxygen atoms
0 1 2 3
P600
H/C
N/C
0
0.5
1
1.5
2
2.5
3
0
1
2
3
4
5

437

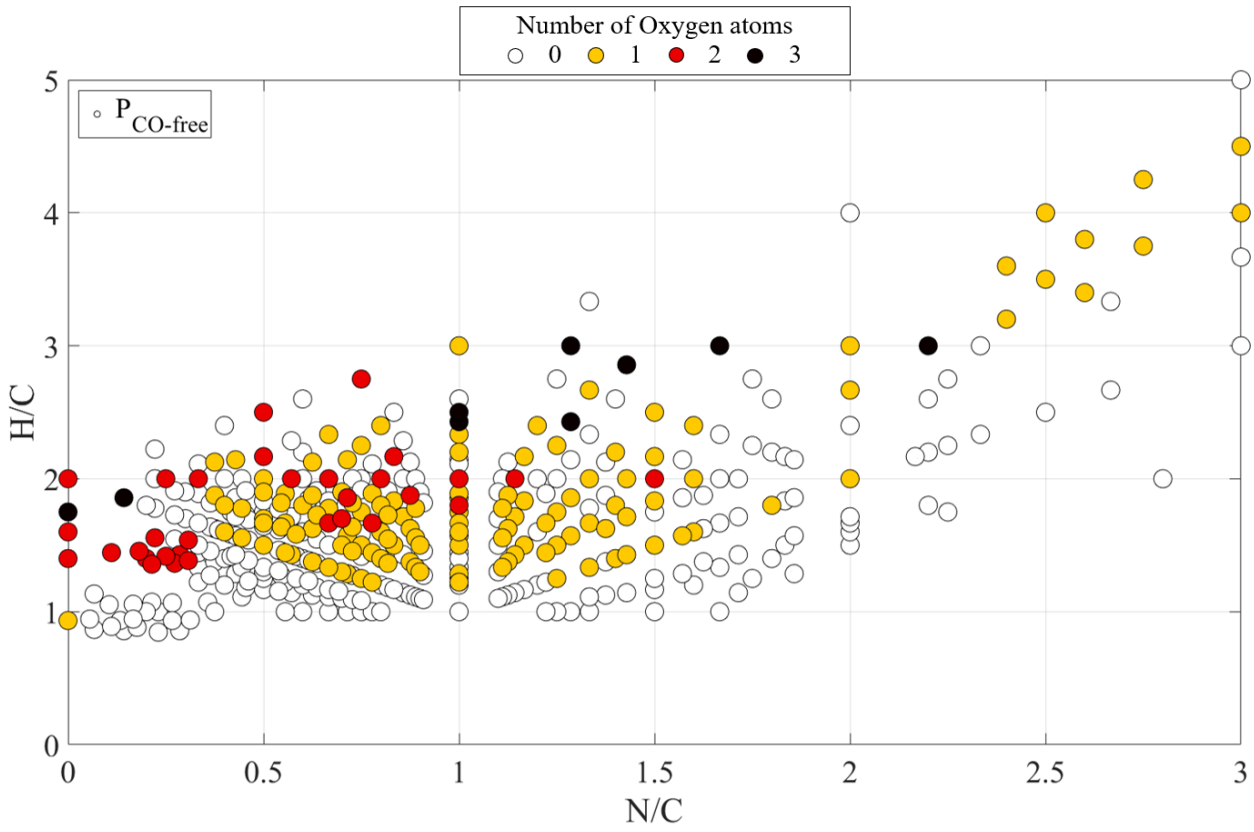

Figure 6: Modified van Krevelen diagrams. The samples were analyzed with the ESI+/Orbitrap technique and the molecules were identified with *Attributor* software. Each dot corresponds to a specific molecule characterized by its Hydrogen-to-Carbon (H/C) and Nitrogen-to-Carbon (N/C) ratios. The colors correspond to the number of oxygen atoms included in the molecules: White ⇔ Zero O atom; Yellow ⇔ One O atom; Red ⇔ Two O atoms; Black ⇔ Three O atoms. Top: P_{400} sample. Middle: P_{600} sample. Bottom: $P_{CO\text{-}free}$ sample.

In Figures 6.top, middle and bottom, we notice that the molecules with one oxygen atom (yellow dots) are scattered all over the distribution for the samples P_{400}, P_{600} and $P_{CO\text{-}free}$. This means that incorporating one atom of oxygen in a molecule does not depend on its nature (light or heavy, low or high H/C and N/C ratios). The second important point is that the oxygenated molecules due to contamination in $P_{CO\text{-}free}$ sample essentially correspond to molecules with one oxygen atom. Thus, the molecules with two and three oxygen atoms (red and black dots, respectively), that are abundantly detected in the soluble fraction of P_{400} and P_{600} samples, are very likely produced by CO chemistry. These molecules are mainly present in a specific area of the diagrams, characterized by the following elemental ratios: [1 < H/C < 2.5 and 0 < N/C < 1]. The fact that N/C ratio is lower than one suggests that the incorporation of more than one oxygen atom in the molecules constituents of the aerosols is done at the expense of nitrogen incorporation. There may be a competition between N_2 and CO chemistries, as suggested by He et al. (2017). The presence of molecules with two or three oxygen atoms at N/C ratio of less than one could also be explained by the incorporation of O atoms into the molecules in the form of carbonyl –C=O or carboxyl –COOH chemical functions. The incorporation of oxygen with carbon into a molecule would therefore necessarily decrease the N/C ratio.

Figure 7 presents the modified van Krevelen diagrams of molecules that are exclusively detected in either the P_{400} (top) or P_{600} (bottom) sample. In Figure 7.top and bottom, we can see

that the molecules specific to P_{400}, oxygenated or not, are scattered all over the distribution, whereas in the sample P_{600}, the molecules group into two distinct areas, suggesting again different reactive pathways for both samples. The area [1 < H/C < 2.5 and 0 < N/C < 1] is composed of a patchwork of heavier molecules including or not oxygen atoms (white, yellow, red and black dots), while the area [2 < H/C < 5 and 1.25 < N/C < 3] is essentially composed of lighter molecules with one oxygen atom (essentially yellow dots). This reinforces the idea that when the percentage of methane increases, the mixing ratio of molecular nitrogen decreases, while there is likely competition between CO and N_2 chemistries (He et al., 2017). Incorporating more than one oxygen atom in heavier molecules, probably in the form of chemical functions –C=O or –COOH, is done at the expense of N-incorporation.

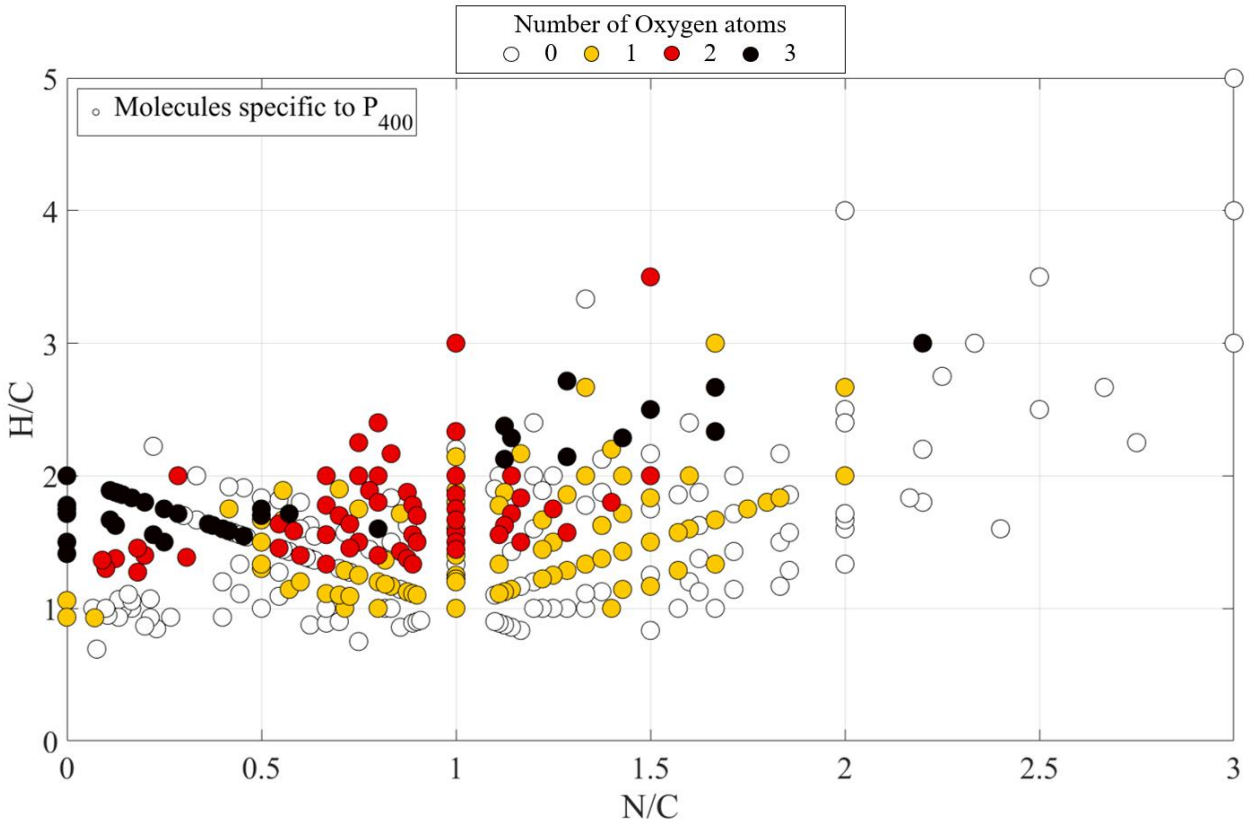

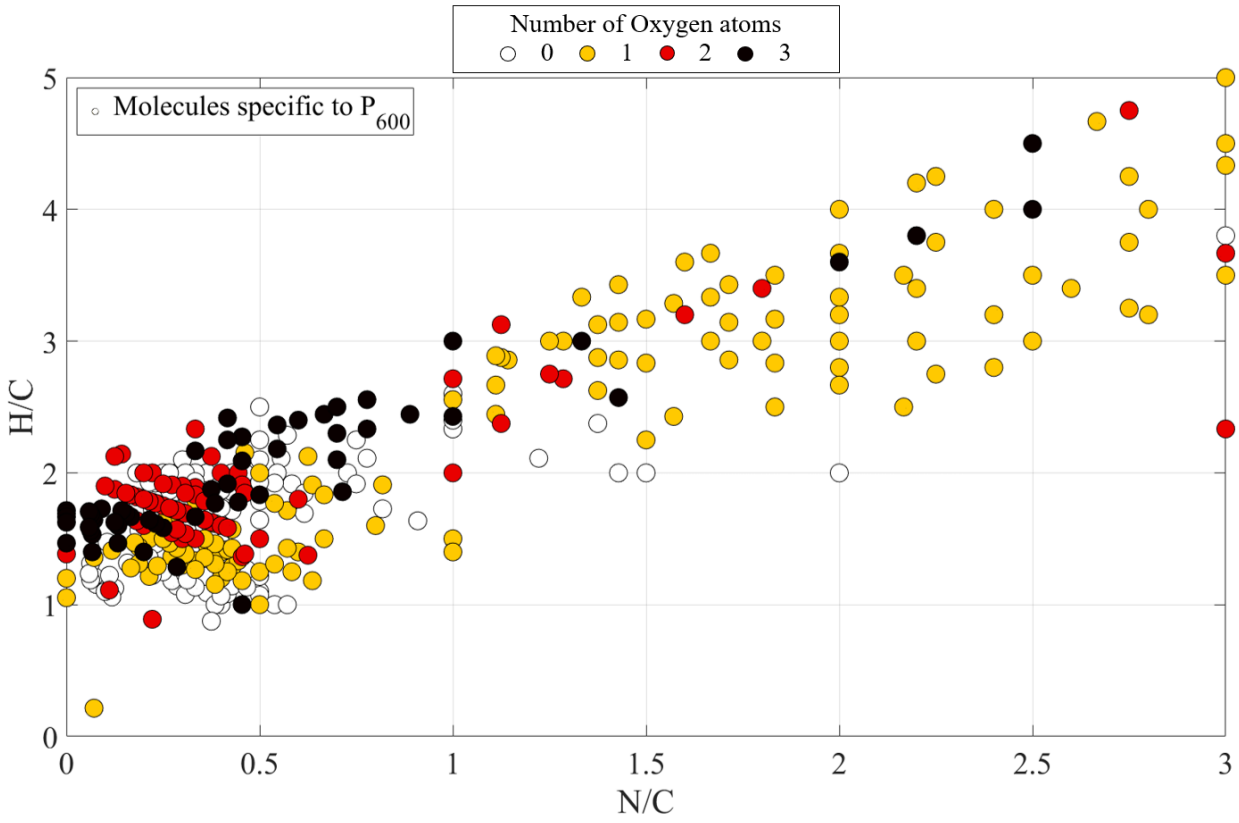

Figure 7: Modified van Krevelen diagrams of the molecules exclusively detected in the soluble fraction of P_{400} (top) and P_{600} (bottom) samples. The samples were analyzed with the ESI+/Orbitrap technique and the molecules were identified with *Attributor* software. Each dot corresponds to a specific molecule characterized by its Hydrogen-to-Carbon (H/C) and Nitrogen-to-Carbon (N/C) ratios. The colors correspond to the number of oxygen atoms included in the molecules: White ⇔ Zero O atom; Yellow ⇔ One O atom; Red ⇔ Two O atoms; Black ⇔ Three O atoms.

In Gautier et al. (2014), a high-resolution mass spectrometry study was carried out on Titan aerosol analogues produced with the PAMPRE experimental setup. This study showed the impact on the molecular composition of Titan aerosol analogues when the methane percentage varies. In particular, there are less molecules formed with N/C < 1 when the percentage of methane increases.

Previous studies have also shown that when CH_4 percentage increases, more hydrogen is available in the gas phase leading to the aerosols, and that this hydrogen tends to inhibit the growth of the aerosol analogues (DeWitt et al., 2009; Sciamma-O'Brien et al., 2010). We can exclude this to be the case here since we do not see a depletion of the "N/C < 1" molecules in the P_{600} sample. This suggests that N_2 and CH_4 chemistry is strongly impacted by the presence of CO, even in a small proportion. Hörst and Tolbert (2014) and He et al. (2017) also studied the effect of carbon monoxide on planetary atmospheric chemistry and on the formation of aerosol analogues and proposed two hypotheses: (1) in presence of carbon monoxide, oxygen radicals coming from CO react with atomic and molecular hydrogen coming from CH_4 and removes them from the chemical system; (2) in presence of CO, there is more carbon available without increasing the quantity of available hydrogen that inhibits the aerosols growth, resulting in a less reducing environment allowing the production of more unsaturated molecules. According to our results, the first hypothesis of Hörst and Tolbert (2014) and He et al. (2017)

may be an explanation to the lack of depletion of the molecules with N/C < 1 when the CH_4 percentage increases. On the contrary, the second hypothesis cannot explain our results. On one hand, the sample P_{600} presents more molecules with higher N/C (and H/C) ratios than P_{400}, meaning that less carbon is incorporated in these molecules. On the other hand, as shown in Figure 4, the soluble fraction of P_{600} contains more unsaturated molecules than that of the P_{400} sample, even though the sample P_{600} is produced with a lower CO/CH_4 ratio.

IV. Discussion

Long before the *New Horizons* era, the photochemical models of Pluto atmosphere scarcely took into consideration N_2 and CO chemistries (Krasnopolsky and Cruikshank, 1999; Lara et al., 1997; Stansberry et al., 1989). It was thought that the formation of the aerosols would be essentially driven by the photolysis of CH_4 by Lyman-α photons. This was also the case on Titan before the *Cassini-Huygens* mission that revealed that not only methane, but also molecular nitrogen plays a key role in Titan atmospheric chemistry and in the formation of N-bearing organic aerosols. In light of this discovery, the latest photochemical models of Pluto atmosphere compensated this misconception by including the chemistry from N_2, but the question of the CO chemistry still remains unsolved (Luspay-Kuti et al., 2017; Wong et al., 2017). CO serves as a source of oxygen for incorporation in haze particles, leading to the formation of prebiotic molecules in the aerosols. This was pointed out by Hörst et al. (2012) who detected amino acids and nucleotide bases in the solid products produced with the PAMPRE experimental setup in a plasma of N_2:CH_4:CO gas mixture. However, even Titan aerosol analogues studies usually do not include CO despite its substantial mixing ratio (47 ± 8 ppm_V) in the hazy atmosphere of Titan (de Kok et al., 2007). Additionally, few studies on exoplanetary atmospheres also emphasized the link between the presence of carbon monoxide and haze layers (Barman et al., 2015; Deming et al., 2013; He et al., 2018a, 2018b; Hörst et al., 2018a; Konopacky et al., 2013; Pont et al., 2013).

For Pluto, an endeavor has recently been done by Luspay-Kuti et al. (2017) and Krasnopolsky, (2020) to incorporate the most important reactions of CO chemistry in their models. Our results obtained by elemental composition analysis highlight an important incorporation of both nitrogen and oxygen atoms in the molecules constituting Pluto aerosol analogues and thus active N_2 and CO chemistries influencing the gas phase composition and density. We thus strongly advise to keep focusing on the effect of CO in Pluto atmospheric chemistry and make sure to include extensive oxygen and nitrogen reactive pathways in future Pluto photochemical models.

From our analyses, we conclude that the molecules constituting the soluble fraction of Pluto aerosol analogues are mainly composed of N-bearing organic molecules, with a significant proportion of oxygenated molecules. Unsaturated molecules may also be present in large amount. These heavy, unsaturated N-bearing organic molecules and oxygenated species are likely very reactive and may therefore catalyze and self-sustain the synthesis of other molecules constituting the aerosols. Furthermore, by interacting with molecules in the gas phase, they may also act as cloud condensation nuclei (Broekhuizen et al., 2004; Fan et al., 2016; Kumar et al., 2003; Lavvas et al., 2016; Luspay-Kuti et al., 2017), impacting the climate of Pluto. Seven

Pluto clouds candidates have been identified by Stern et al. (2017) from *New Horizons* image dataset. These clouds could be the result of the condensation of HCN, C_2H_2, C_2H_6, C_2H_4 or CH_4. One interesting question is whether the condensation of clouds on Pluto aerosols is affected by the proportion of O-bearing molecules in the hazes. The study of the wettability of Pluto aerosol analogues to HCN, C_2H_2, C_2H_6, C_2H_4 or CH_4 may provide answers to this question.

Pluto atmosphere is around 30 K colder than theoretically predicted, at about 400 km of altitude (Gladstone et al., 2016; Zhang et al., 2017; Zhu et al., 2014). Because of Pluto thermal structure, expected to be in radiative-conductive equilibrium, atmospheric gas molecules such as HCN or water vapor are not sufficient to explain Pluto temperature profile. Zhang et al. (2017) proposed that Pluto haze, rather than its atmospheric gases, could explain Pluto cold atmosphere. Their study was performed using the optical properties of Titan aerosol analogues, which are oxygen-free. Our results obtained by elemental composition analysis and ESI+/Orbitrap showed a significant incorporation of oxygen atoms in the molecules constituting Pluto aerosol analogues and that this O-incorporation depends on CH_4 mixing ratio. As more oxygen is incorporated, the real and imaginary refractive indices of haze particles change, resulting in different optical properties that may reduce UV wavelengths from reaching Pluto surface and influence Pluto radiative cooling. While Zhang et al. (2017) showed a dependency of Pluto climate to the aerosols simulated optical constants, Gavilan et al. (2017) have shown that when the percentage of oxygen increases in organic aerosols, the absorption at longer UV wavelengths is significantly higher. The experimental determination of the UV-Visible refractive indices of Pluto aerosol analogues is thus of prime importance to further advance our understanding of Pluto cold atmosphere.

V. Conclusion

In this study, we produced Pluto aerosol analogues using the PAMPRE experimental setup. The sample P_{400} is expected to be representative of aerosols that form at 400 km of altitude in Pluto atmosphere. The sample P_{600} is an analogue of aerosols that could form at 600 km of altitude. To determine the chemical composition of these analogues of Pluto aerosols, we performed infrared spectroscopy and elemental composition analyses on them. The samples were also analyzed using very high-resolution mass spectrometry, with the ESI+/Orbitrap technique. Our results show:

(1) Substantial incorporation of nitrogen atoms in Pluto aerosol analogues: nitrogen accounts for about 36 and 45 % in mass of Pluto aerosol analogues P_{600} and P_{400}, respectively. The N-bearing chemical functions essentially correspond to primary and secondary amines –NH and $–NH_2$, C=N double bonds in aromatic and hetero-aromatic cycles, nitriles –C≡N, isocyanides –N≡C and carbodiimides –N=C=N–.
(2) A significant proportion of O-bearing molecules is formed by chemistry of CO: about 1.9 and 1.7 % of oxygen in mass in samples P_{400} and P_{600}, respectively.
(3) An impact of methane percentage – and thus the altitude of aerosols formation on Pluto – on the chemical composition of the aerosols. This impact strongly affects the nitrogen and oxygen contents of the hazes. In particular, we show that the bulk sample of aerosols produced at low altitude (P_{400}) contains more nitrogen and oxygen than the bulk sample of aerosols produced at high altitude (P_{600}).

Pluto aerosols have a strong impact on Pluto climate, acting as condensation nuclei or affecting the atmosphere radiative balance (Luspay-Kuti et al., 2017; Zhang et al., 2017). However, these exact interactions are still poorly understood and further experimental work is needed on the aerosols-gas interactions and the aerosols optical properties to further refine Pluto atmospheric models.

Finally, Sebree et al. (2018) have recently detected prebiotic molecules in aerosols formed from an AC glow discharge in a N_2:CH_4:CO gas mixture with a high CO mixing ratio, and a recent review was also published by Cruikshank et al. (2019) about the implications of Pluto for the prebiotic chemistry. In our data, we detected at *m/z* 111.043 the following chemical formula $C_4H_5N_3O$, which can correspond to cytosine, the easiest produced nucleobase. To confirm the presence of this biomolecule in Pluto aerosol analogues, it would be necessary to analyze them by chromatography coupled to mass spectrometry, in order to get structural information of the molecules.

Acknowledgements

We are grateful to the European Research Council Starting Grant *PrimChem* for funding this work (grant agreement n° 636829).

References

Alcouffe, G., Cavarroc, M., Cernogora, G., Ouni, F., Jolly, A., Boufendi, L., Szopa, C., 2009. Capacitively coupled plasma used to simulate Titan's atmospheric chemistry. Plasma Sources Sci. Technol. 19, 15008. https://doi.org/10.1088/0963-0252/19/1/015008

Anicich, V.G., Wilson, P., McEwan, M.J., 2003. Termolecular ion-molecule reactions in Titan's atmosphere. IV. A search made at up to 1 micron in pure hydrocarbons. J. Am. Soc. Mass Spectrom. 14, 900–915. https://doi.org/10.1016/S1044-0305(03)00218-6

Banks, J.F., Whitehouse, C.M., 1996. Electrospray Ionization Mass Spectrometry. Methods Enzymol. 270, 486–519. https://doi.org/10.1016/s0076-6879(96)70023-x

Barman, T.S., Konopacky, Q.M., Macintosh, B., Marois, C., 2015. Simultaneous Detection of Water, Methane and Carbon Monoxide in the Atmosphere of Exoplanet HR 8799 b. Astrophys. J. 804, 61. https://doi.org/10.1088/0004-637x/804/1/61

Böhme, D.K., 2000. Experimental studies of positive ion chemistry with flow-tube mass spectrometry: birth, evolution, and achievements in the 20th century. Int. J. Mass Spectrom. 200, 97–136. https://doi.org/https://doi.org/10.1016/S1387-3806(00)00299-2

Broekhuizen, K.E., Thornberry, T., Kumar, P.P., Abbatt, J.P.D., 2004. Formation of cloud condensation nuclei by oxidative processing: Unsaturated fatty acids. J. Geophys. Res. Atmos. 109. https://doi.org/10.1029/2004JD005298

Cable, M.L., Hörst, S.M., Hodyss, R., Beauchamp, P.M., Smith, M.A., Willis, P.A., 2012. Titan Tholins: Simulating Titan Organic Chemistry in the Cassini-Huygens Era. Chem. Rev. 112, 1882–1909. https://doi.org/10.1021/cr200221x

Carrasco, N., Gautier, T., Es-sebbar, E., Pernot, P., Cernogora, G., 2012. Volatile products controlling Titan's tholins production. Icarus 219, 230–240. https://doi.org/https://doi.org/10.1016/j.icarus.2012.02.034

Carrasco, N., Jomard, F., Vigneron, J., Etcheberry, A., Cernogora, G., 2016. Laboratory analogues simulating Titan's atmospheric aerosols: Compared chemical compositions of grains and thin films. Planet. Space Sci. 128, 52–57. https://doi.org/https://doi.org/10.1016/j.pss.2016.05.006

Carrasco, N., Schmitz-Afonso, I., Bonnet, J.-Y., Quirico, E., Thissen, R., Dutuit, O., Bagag, A., Laprévote, O., Buch, A., Giuliani, A., Adandé, G., Ouni, F., Hadamcik, E., Szopa, C., Cernogora, G., 2009. Chemical Characterization of Titan's Tholins: Solubility, Morphology and Molecular Structure Revisited. J. Phys. Chem. A 113, 11195–11203. https://doi.org/10.1021/jp904735q

Cheng, A.F., Summers, M.E., Gladstone, G.R., Strobel, D.F., Young, L.A., Lavvas, P., Kammer, J.A., Lisse, C.M., Parker, A.H., Young, E.F., Stern, S.A., Weaver, H.A., Olkin, C.B., Ennico, K.A., 2017. Haze in Pluto's atmosphere. Icarus 290, 112–133. https://doi.org/https://doi.org/10.1016/j.icarus.2017.02.024

Coll, P., Coscia, D., Smith, N.S., Gazeau, M.-C., Ramírez, S.I., Cernogora, G., Israël, G.,

Raulin, F., 1999. Experimental laboratory simulation of Titan's atmosphere: aerosols and gas phase. Planet. Space Sci. 47, 1331–1340. https://doi.org/https://doi.org/10.1016/S0032-0633(99)00054-9

Coll, P., Navarro-González, R., Szopa, C., Poch, O., Ramírez, S.I., Coscia, D., Raulin, F., Cabane, M., Buch, A., Israël, G., 2013. Can laboratory tholins mimic the chemistry producing Titan's aerosols? A review in light of ACP experimental results. Planet. Space Sci. 77, 91–103. https://doi.org/https://doi.org/10.1016/j.pss.2012.07.006

Cruikshank, D.P., Materese, C.K., Pendleton, Y.J., Boston, P.J., Grundy, W.M., Schmitt, B., Lisse, C.M., Runyon, K.D., Keane, J.T., Beyer, R.A., Summers, M.E., Scipioni, F., Stern, S.A., Dalle Ore, C.M., Olkin, C.B., Young, L.A., Ennico, K.A., Weaver, H.A., Bray, V.J., 2019. Prebiotic Chemistry of Pluto. Astrobiology 19, 831–848. https://doi.org/10.1089/ast.2018.1927

Danger, G., Fresneau, A., Abou Mrad, N., de Marcellus, P., Orthous-Daunay, F.-R., Duvernay, F., Vuitton, V., Le Sergeant d'Hendecourt, L., Thissen, R., Chiavassa, T., 2016. Insight into the molecular composition of laboratory organic residues produced from interstellar/pre-cometary ice analogues using very high resolution mass spectrometry. Geochim. Cosmochim. Acta 189, 184–196. https://doi.org/https://doi.org/10.1016/j.gca.2016.06.014

de Kok, R., Irwin, P.G.J., Teanby, N.A., Lellouch, E., Bézard, B., Vinatier, S., Nixon, C.A., Fletcher, L., Howett, C.J.A., Calcutt, S.B., Bowles, N.E., Flasar, F.M., Taylor, F.W., 2007. Oxygen compounds in Titan's stratosphere as observed by Cassini CIRS. Icarus 186, 354–363. https://doi.org/https://doi.org/10.1016/j.icarus.2006.09.016

Decker, C., Jenkins, A.D., 1985. Kinetic approach of oxygen inhibition in ultraviolet- and laser-induced polymerizations. Macromolecules 18, 1241–1244. https://doi.org/10.1021/ma00148a034

Deming, D., Wilkins, A., McCullough, P., Crouzet, N., Burrows, A., Fortney, J.J., Agol, E., Dobbs-Dixon, I., Madhusudhan, N., Desert, J.-M., Knutson, H.A., Line, M., Gilliland, R.L., Haynes, K., Magic, Z., Mandell, A.M., Clampin, M., Ranjan, S., Charbonneau, D., Seager, S., 2013. Infrared Transmission Spectroscopy of the Exoplanets HD 209458b and XO-1b using the Wide Field Camera-3 on the Hubble Space Telescope. Astrophys. J. 774, 17. https://doi.org/DOI:101088/0004-637X/774/2/95

Derenne, S., Coelho, C., Anquetil, C., Szopa, C., Rahman, A.S., McMillan, P.F., Corà, F., Pickard, C.J., Quirico, E., Bonhomme, C., 2012. New insights into the structure and chemistry of Titan's tholins via 13C and 15N solid state nuclear magnetic resonance spectroscopy. Icarus 221, 844–853. https://doi.org/https://doi.org/10.1016/j.icarus.2012.03.003

DeWitt, H.L., Trainer, M.G., Pavlov, A.A., Hasenkopf, C.A., Aiken, A.C., Jimenez, J.L., McKay, C.P., Toon, O.B., Tolbert, M.A., 2009. Reduction in Haze Formation Rate on Prebiotic Earth in the Presence of Hydrogen. Astrobiology 9, 447–453. https://doi.org/10.1089/ast.2008.0289

Dubois, D., Carrasco, N., Petrucciani, M., Vettier, L., Tigrine, S., Pernot, P., 2019. In situ investigation of neutrals involved in the formation of Titan tholins. Icarus 317, 182–196. https://doi.org/https://doi.org/10.1016/j.icarus.2018.07.006

Elliot, J.L., Dunham, E.W., Bosh, A.S., Slivan, S.M., Young, L.A., Wasserman, L.H., Millis, R.L., 1989. Pluto's atmosphere. Icarus 77, 148–170. https://doi.org/https://doi.org/10.1016/0019-1035(89)90014-6

Fan, J., Wang, Y., Rosenfeld, D., Liu, X., 2016. Review of Aerosol-Cloud Interactions: Mechanisms, Significance, and Challenges. J. Atmos. Sci. 73, 4221–4252. https://doi.org/10.1175/JAS-D-16-0037.1

Fleury, B., Carrasco, N., Gautier, T., Mahjoub, A., He, J., Szopa, C., Hadamcik, E., Buch, A., Cernogora, G., 2014. Influence of CO on Titan atmospheric reactivity. Icarus 238, 221–229. https://doi.org/https://doi.org/10.1016/j.icarus.2014.05.027

Forget, F., Bertrand, T., Vangvichith, M., Leconte, J., Millour, E., Lellouch, E., 2017. A post-New Horizons global climate model of Pluto including the N2, CH4 and CO cycles. Icarus 287, 54–71. https://doi.org/https://doi.org/10.1016/j.icarus.2016.11.038

Gao, P., Fan, S., Wong, M.L., Liang, M.-C., Shia, R.-L., Kammer, J.A., Yung, Y.L., Summers, M.E., Gladstone, G.R., Young, L.A., Olkin, C.B., Ennico, K.A., Weaver, H.A., Stern, S.A., 2017. Constraints on the microphysics of Pluto's photochemical haze from New Horizons observations. Icarus 287, 116–123. https://doi.org/https://doi.org/10.1016/j.icarus.2016.09.030

Gautier, T., Carrasco, N., Buch, A., Szopa, C., Sciamma-O'Brien, E., Cernogora, G., 2011. Nitrile gas chemistry in Titan's atmosphere. Icarus 213, 625–635. https://doi.org/https://doi.org/10.1016/j.icarus.2011.04.005

Gautier, T., Carrasco, N., Mahjoub, A., Vinatier, S., Giuliani, A., Szopa, C., Anderson, C.M., Correia, J.-J., Dumas, P., Cernogora, G., 2012. Mid- and far-infrared absorption spectroscopy of Titan's aerosols analogues. Icarus 221, 320–327. https://doi.org/https://doi.org/10.1016/j.icarus.2012.07.025

Gautier, T., Carrasco, N., Schmitz-Afonso, I., Touboul, D., Szopa, C., Buch, A., Pernot, P., 2014. Nitrogen incorporation in Titan's tholins inferred by high resolution orbitrap mass spectrometry and gas chromatography–mass spectrometry. Earth Planet. Sci. Lett. 404, 33–42. https://doi.org/https://doi.org/10.1016/j.epsl.2014.07.011

Gautier, T., Schmitz-Afonso, I., Touboul, D., Szopa, C., Buch, A., Carrasco, N., 2016. Development of HPLC-Orbitrap method for identification of N-bearing molecules in complex organic material relevant to planetary environments. Icarus 275, 259–266. https://doi.org/https://doi.org/10.1016/j.icarus.2016.03.007

Gautier, T., Sebree, J.A., Li, X., Pinnick, V.T., Grubisic, A., Loeffler, M.J., Getty, S.A., Trainer, M.G., Brinckerhoff, W.B., 2017. Influence of trace aromatics on the chemical growth mechanisms of Titan aerosol analogues. Planet. Space Sci. 140, 27–34. https://doi.org/https://doi.org/10.1016/j.pss.2017.03.012

Gavilan, L., Broch, L., Carrasco, N., Fleury, B., Vettier, L., 2017. Organic Aerosols in the Presence of CO2 in the Early Earth and Exoplanets: UV–Vis Refractive Indices of Oxidized Tholins. Astrophys. J. 848, L5. https://doi.org/10.3847/2041-8213/aa8cc4

Gladstone, G.R., Pryor, W.R., Stern, S.A., 2015. Lyα@Pluto. Icarus 246, 279–284. https://doi.org/https://doi.org/10.1016/j.icarus.2014.04.016

Gladstone, G.R., Stern, S.A., Ennico, K.A., Olkin, C.B., Weaver, H.A., Young, L.A., Summers, M.E., Strobel, D.F., Hinson, D.P., Kammer, J.A., Parker, A.H., Steffl, A.J., Linscott, I.R., Parker, J.W., Cheng, A.F., Slater, D.C., Versteeg, M.H., Greathouse, T.K., Retherford, K.D., Throop, H.B., Cunningham, N.J., Woods, W.W., Singer, K.N., Tsang, C.C.C., Schindhelm, E., Lisse, C.M., Wong, M.L., Yung, Y.L., Zhu, X., Curdt, W., Lavvas, P., Young, E.F., Tyler, G.L., 2016. The atmosphere of Pluto as observed by New Horizons. Science (80-.). 351.

Gladstone, G.R., Young, L.A., 2019. New Horizons Observations of the Atmosphere of Pluto. Annu. Rev. Earth Planet. Sci. 47, 119–140. https://doi.org/10.1146/annurev-earth-053018-060128

Grundy, W.M., Binzel, R.P., Buratti, B.J., Cook, J.C., Cruikshank, D.P., Dalle Ore, C.M., Earle, A.M., Ennico, K.A., Howett, C.J.A., Lunsford, A.W., Olkin, C.B., Parker, A.H., Philippe, S., Protopapa, S., Quirico, E., Reuter, D.C., Schmitt, B., Singer, K.N., Verbiscer, A.J., Beyer, R.A., Buie, M.W., Cheng, A.F., Jennings, D.E., Linscott, I.R., Parker, J.W., Schenk, P.M., Spencer, J.R., Stansberry, J.A., Stern, S.A., Throop, H.B., Tsang, C.C.C., Weaver, H.A., Weigle, G.E., Young, L.A., 2016. Surface compositions across Pluto and Charon. Science (80-.). 351.

He, C., Hörst, S.M., Lewis, N.K., Yu, X., Moses, J.I., Kempton, E.M.-R., Marley, M.S., McGuiggan, P., Morley, C. V., Valenti, J.A., Vuitton, V., 2018a. Photochemical Haze Formation in the Atmospheres of Super-Earths and Mini-Neptunes. Astron. J. 156, 38. https://doi.org/10.3847/1538-3881/aac883

He, C., Hörst, S.M., Lewis, N.K., Yu, X., Moses, J.I., Kempton, E.M.-R., McGuiggan, P., Morley, C. V., Valenti, J.A., Vuitton, V., 2018b. Laboratory Simulations of Haze Formation in the Atmospheres of Super-Earths and Mini-Neptunes: Particle Color and Size Distribution. Astrophys. J. 856, L3. https://doi.org/10.3847/2041-8213/aab42b

He, C., Hörst, S.M., Riemer, S., Sebree, J.A., Pauley, N., Vuitton, V., 2017. Carbon Monoxide Affecting Planetary Atmospheric Chemistry. Astrophys. J. 841, L31. https://doi.org/10.3847/2041-8213/aa74cc

He, C., Smith, M.A., 2014. Identification of nitrogenous organic species in Titan aerosols analogs: Implication for prebiotic chemistry on Titan and early Earth. Icarus 238, 86–92. https://doi.org/https://doi.org/10.1016/j.icarus.2014.05.012

He, C., Smith, M.A., 2013. Identification of nitrogenous organic species in Titan aerosols analogs: Nitrogen fixation routes in early atmospheres. Icarus 226, 33–40. https://doi.org/https://doi.org/10.1016/j.icarus.2013.05.013

Hinson, D.P., Linscott, I.R., Young, L.A., Tyler, G.L., Stern, S.A., Beyer, R.A., Bird, M.K., Ennico, K.A., Gladstone, G.R., Olkin, C.B., Pätzold, M., Schenk, P.M., Strobel, D.F., Summers, M.E., Weaver, H.A., Woods, W.W., 2017. Radio occultation measurements of Pluto's neutral atmosphere with New Horizons. Icarus 290, 96–111. https://doi.org/https://doi.org/10.1016/j.icarus.2017.02.031

Hörst, S.M., He, C., Lewis, N.K., Kempton, E.M.-R., Marley, M.S., Morley, C. V., Moses, J.I., Valenti, J.A., Vuitton, V., 2018a. Haze production rates in super-Earth and mini-Neptune atmosphere experiments. Nat. Astron. 2, 303–306. https://doi.org/10.1038/s41550-018-0397-0

Hörst, S.M., Tolbert, M.A., 2014. The Effect of Carbon Monoxide on Planetary Haze Formation. Astrophys. J. 781, 53. https://doi.org/10.1088/0004-637x/781/1/53

Hörst, S.M., Yelle, R. V., Buch, A., Carrasco, N., Cernogora, G., Dutuit, O., Quirico, E., Sciamma-O'Brien, E., Smith, M.A., Somogyi, Á., Szopa, C., Thissen, R., Vuitton, V., 2012. Formation of Amino Acids and Nucleotide Bases in a Titan Atmosphere Simulation Experiment. Astrobiology 12, 809–817. https://doi.org/10.1089/ast.2011.0623

Hörst, S.M., Yoon, Y.H., Ugelow, M.S., Parker, A.H., Li, R., de Gouw, J.A., Tolbert, M.A., 2018b. Laboratory investigations of Titan haze formation: In situ measurement of gas and particle composition. Icarus 301, 136–151. https://doi.org/https://doi.org/10.1016/j.icarus.2017.09.039

Hubbard, W.B., Hunten, D.M., Dieters, S.W.B., Hill, K.M., Watson, R.D., 1988. Occultation evidence for an atmosphere on Pluto. Nature 336, 452.

Imanaka, H., Khare, B.N., Elsila, J.E., Bakes, E.L.O., McKay, C.P., Cruikshank, D.P., Sugita, S., Matsui, T., Zare, R.N., 2004. Laboratory experiments of Titan tholin formed in cold plasma at various pressures: Implications for nitrogen-containing polycyclic aromatic compounds in Titan haze. Icarus 168, 344–366. https://doi.org/https://doi.org/10.1016/j.icarus.2003.12.014

Imanaka, H., Smith, M.A., 2010. Formation of nitrogenated organic aerosols in the Titan upper atmosphere. Proc. Natl. Acad. Sci. U. S. A. 107, 12423–12428. https://doi.org/10.1073/pnas.0913353107

Imanaka, H., Smith, M.A., 2009. EUV Photochemical Production of Unsaturated Hydrocarbons: Implications to EUV Photochemistry in Titan and Jovian Planets. J. Phys. Chem. A 113, 11187–11194. https://doi.org/10.1021/jp9041952

Khare, B.N., Sagan, C., Thompson, W.R., Arakawa, E.T., Suits, F., Callcott, T.A., Williams, M.W., Shrader, S., Ogino, H., Willingham, T.O., Nagy, B., 1984. The organic aerosols of Titan. Adv. Sp. Res. 4, 59–68. https://doi.org/https://doi.org/10.1016/0273-1177(84)90545-3

Kim, S., Kramer, R.W., Hatcher, P.G., 2003. Graphical Method for Analysis of Ultrahigh-Resolution Broadband Mass Spectra of Natural Organic Matter, the Van Krevelen

Diagram. Anal. Chem. 75, 5336–5344. https://doi.org/10.1021/ac034415p

Konopacky, Q.M., Barman, T.S., Macintosh, B.A., Marois, C., 2013. Detection of Carbon Monoxide and Water Absorption Lines in an Exoplanet Atmosphere. Science (80-.). 339, 1398–1401. https://doi.org/10.1126/science.1232003

Krasnopolsky, V.A., 2020. A photochemical model of Pluto's atmosphere and ionosphere. Icarus 335, 113374. https://doi.org/https://doi.org/10.1016/j.icarus.2019.07.008

Krasnopolsky, V.A., Cruikshank, D.P., 1999. Photochemistry of Pluto's atmosphere and ionosphere near perihelion. J. Geophys. Res. Planets 104, 21979–21996. https://doi.org/10.1029/1999JE001038

Kumar, P.P., Broekhuizen, K.E., Abbatt, J.P.D., 2003. Organic acids as cloud condensation nuclei: Laboratory studies of highly soluble and insoluble species. Atmos. Chem. Phys. 3, 509–520. https://doi.org/10.5194/acp-3-509-2003

Lara, L.M., Ip, W., Rodrigo, R., 1997. Photochemical Models of Pluto's Atmosphere. Icarus 130, 16–35. https://doi.org/https://doi.org/10.1006/icar.1997.5798

Lavvas, P., Strobel, D.F., Lellouch, E., Gurwell, M.A., Cheng, A.F., Summers, M., Gladstone, G.R., 2016. Photochemical aerosol formation in planetary atmospheres: A comparison between Pluto and Titan, in: AAS/Division for Planetary Sciences Meeting Abstracts #48. p. 224.06.

Lellouch, E., 1994. The Thermal Structure of Pluto's Atmosphere: Clear vs. Hazy Models. Icarus 108, 255–264. https://doi.org/https://doi.org/10.1006/icar.1994.1060

Lellouch, E., Gurwell, M.A., Butler, B.J., Fouchet, T., Lavvas, P., Strobel, D.F., Sicardy, B., Moullet, A., Moreno, R., Bockelée-Morvan, D., Biver, N., Young, L.A., Lis, D.C., Stansberry, J.A., Stern, S.A., Weaver, H.A., Young, E.F., Zhu, X., Boissier, J., 2017. Detection of CO and HCN in Pluto's atmosphere with ALMA. Icarus 286, 289–307. https://doi.org/https://doi.org/10.1016/j.icarus.2016.10.013

Ligon, S.C., Husár, B., Wutzel, H., Holman, R., Liska, R., 2014. Strategies to Reduce Oxygen Inhibition in Photoinduced Polymerization. Chem. Rev. 114, 557–589. https://doi.org/10.1021/cr3005197

Luspay-Kuti, A., Mandt, K., Jessup, K.L., Kammer, J., Hue, V., Hamel, M., Filwett, R., 2017. Photochemistry on Pluto: Part I. Hydrocarbons and aerosols. Mon. Not. R. Astron. Soc. 472, 104–117. https://doi.org/10.1093/mnras/stx1362

Maillard, J., Carrasco, N., Schmitz-Afonso, I., Gautier, T., Afonso, C., 2018. Comparison of soluble and insoluble organic matter in analogues of Titan's aerosols. Earth Planet. Sci. Lett. 495, 185–191. https://doi.org/https://doi.org/10.1016/j.epsl.2018.05.014

Makarov, A., Denisov, E., Kholomeev, A., Balschun, W., Lange, O., Strupat, K., Horning, S., 2006. Performance Evaluation of a Hybrid Linear Ion Trap/Orbitrap Mass Spectrometer. Anal. Chem. 78, 2113–2120. https://doi.org/10.1021/ac0518811

834 Mandt, K., Luspay-Kuti, A., Hamel, M., Jessup, K.-L., Hue, V., Kammer, J.A., Filwett, R.,
835 2017. Photochemistry on Pluto: Part II. HCN and nitrogen isotope fractionation. Mon.
836 Not. R. Astron. Soc. 472, 118–128. https://doi.org/10.1093/mnras/stx1587

837 Marshall, A.G., Rodgers, R.P., 2008. Petroleomics: Chemistry of the underworld. Proc. Natl.
838 Acad. Sci. 105, 18090–18095. https://doi.org/10.1073/pnas.0805069105

839 McDonald, G.D., Thompson, W.R., Heinrich, M., Khare, B.N., Sagan, C., 1994. Chemical
840 Investigation of Titan and Triton Tholins. Icarus 108, 137–145.
841 https://doi.org/https://doi.org/10.1006/icar.1994.1046

842 Molnárné Guricza, L., Schrader, W., 2015. Electrospray ionization for determination of non-
843 polar polyaromatic hydrocarbons and polyaromatic heterocycles in heavy crude oil
844 asphaltenes. J. Mass Spectrom. 50, 549–557. https://doi.org/10.1002/jms.3561

845 Morisson, M., Szopa, C., Carrasco, N., Buch, A., Gautier, T., 2016. Titan's organic aerosols:
846 Molecular composition and structure of laboratory analogues inferred from pyrolysis gas
847 chromatography mass spectrometry analysis. Icarus 277, 442–454.
848 https://doi.org/https://doi.org/10.1016/j.icarus.2016.05.038

849 Orthous-Daunay, F.-R., Piani, L., Flandinet, L., Thissen, R., Wolters, W., Vuitton, V., Poch,
850 O., Moynier, F., Sugawara, I., Naraoka, H., Tachibana, S., 2019. Ultraviolet-photon
851 fingerprints on chondritic large organic molecules. Geochem. J. 53, 21–32.

852 Owen, T.C., Roush, T.L., Cruikshank, D.P., Elliot, J.L., Young, L.A., de Bergh, C., Schmitt,
853 B., Geballe, T.R., Brown, R.H., Bartholomew, M.J., 1993. Surface Ices and the
854 Atmospheric Composition of Pluto. Science (80-.). 261, 745 LP – 748.

855 Pernot, P., Carrasco, N., Thissen, R., Schmitz-Afonso, I., 2010. Tholinomics - Chemical
856 Analysis of Nitrogen-Rich Polymers. Anal. Chem. 82, 1371–1380.
857 https://doi.org/10.1021/ac902458q

858 Perry, R.H., Cooks, R.G., Noll, R.J., 2008. Orbitrap mass spectrometry: Instrumentation, ion
859 motion and applications. Mass Spectrom. Rev. 27, 661–699.
860 https://doi.org/10.1002/mas.20186

861 Pont, F.J., Sing, D.K., Gibson, N.P., Aigrain, S., Henry, G.W., Husnoo, N., 2013. The
862 prevalence of dust on the exoplanet HD 189733b from Hubble and Spitzer observations.
863 Mon. Not. R. Astron. Soc. 432, 2917–2944. https://doi.org/10.1093/mnras/stt651

864 Rodgers, R.P., Schaub, T.M., Marshall, A.G., 2005. Petroleomics: MS Returns to Its Roots.
865 Anal. Chem. 77, 20–27. https://doi.org/10.1021/ac053302y

866 Sarker, N., Somogyi, Á., Lunine, J.I., Smith, M.A., 2003. Titan Aerosol Analogues: Analysis
867 of the Nonvolatile Tholins. Astrobiology 3, 719–726.
868 https://doi.org/10.1089/153110703322736042

869 Sciamma-O'Brien, E., Carrasco, N., Szopa, C., Buch, A., Cernogora, G., 2010. Titan's
870 atmosphere: An optimal gas mixture for aerosol production? Icarus 209, 704–714.
871 https://doi.org/https://doi.org/10.1016/j.icarus.2010.04.009

Sciamma-O'Brien, E., Upton, K.T., Salama, F., 2017. The Titan Haze Simulation (THS) experiment on COSmIC. Part II. Ex-situ analysis of aerosols produced at low temperature. Icarus 289, 214–226. https://doi.org/https://doi.org/10.1016/j.icarus.2017.02.004

Sebree, J.A., Roach, M.C., Shipley, E.R., He, C., Hörst, S.M., 2018. Detection of Prebiotic Molecules in Plasma and Photochemical Aerosol Analogs Using GC/MS/MS Techniques. Astrophys. J. 865, 133. https://doi.org/10.3847/1538-4357/aadba1

Sekine, Y., Lebonnois, S., Imanaka, H., Matsui, T., Bakes, E.L.O., McKay, C.P., Khare, B.N., Sugita, S., 2008. The role of organic haze in Titan's atmospheric chemistry: II. Effect of heterogeneous reaction to the hydrogen budget and chemical composition of the atmosphere. Icarus 194, 201–211. https://doi.org/https://doi.org/10.1016/j.icarus.2007.08.030

Somogyi, Á., Oh, C.-H., Smith, M.A., Lunine, J.I., 2005. Organic environments on Saturn's moon, Titan: Simulating chemical reactions and analyzing products by FT-ICR and ion-trap mass spectrometry. J. Am. Soc. Mass Spectrom. 16, 850–859. https://doi.org/10.1016/j.jasms.2005.01.027

Somogyi, Á., Smith, M.A., Vuitton, V., Thissen, R., Komáromi, I., 2012. Chemical ionization in the atmosphere? A model study on negatively charged "exotic" ions generated from Titan's tholins by ultrahigh resolution MS and MS/MS. Int. J. Mass Spectrom. 316–318, 157–163. https://doi.org/https://doi.org/10.1016/j.ijms.2012.02.026

Somogyi, Á., Thissen, R., Orthous-Daunay, F.-R., Vuitton, V., 2016. The Role of Ultrahigh Resolution Fourier Transform Mass Spectrometry (FT-MS) in Astrobiology-Related Research: Analysis of Meteorites and Tholins. Int. J. Mol. Sci. https://doi.org/10.3390/ijms17040439

Stansberry, J.A., Lunine, J.I., Tomasko, M.G., 1989. Upper limits on possible photochemical hazes on Pluto. Geophys. Res. Lett. 16, 1221–1224. https://doi.org/10.1029/GL016i011p01221

Stern, S.A., Bagenal, F., Ennico, K.A., Gladstone, G.R., Grundy, W.M., McKinnon, W.B., Moore, J.M., Olkin, C.B., Spencer, J.R., Weaver, H.A., Young, L.A., Andert, T., Andrews, J., Banks, M., Bauer, B., Bauman, J., Barnouin, O.S., Bedini, P., Beisser, K., Beyer, R.A., Bhaskaran, S., Binzel, R.P., Birath, E., Bird, M.K., Bogan, D.J., Bowman, A., Bray, V.J., Brozović, M., Bryan, C., Buckley, M.R., Buie, M.W., Buratti, B.J., Bushman, S.S., Calloway, A., Carcich, B., Cheng, A.F., Conard, S.J., Conrad, C.A., Cook, J.C., Cruikshank, D.P., Custodio, O.S., Dalle Ore, C.M., Deboy, C., Dischner, Z.J.B., Dumont, P., Earle, A.M., Elliott, H.A., Ercol, J., Ernst, C.M., Finley, T., Flanigan, S.H., Fountain, G., Freeze, M.J., Greathouse, T., Green, J.L., Guo, Y., Hahn, M., Hamilton, D.P., Hamilton, S.A., Hanley, J., Harch, A., Hart, H.M., Hersman, C.B., Hill, A., Hill, M.E., Hinson, D.P., Holdridge, M.E., Horányi, M., Howard, A.D., Howett, C.J.A., Jackman, C., Jacobson, R.A., Jennings, D.E., Kammer, J.A., Kang, H.K., Kaufmann, D.E., Kollmann, P., Krimigis, S.M., Kusnierkiewicz, D., Lauer, T.R., Lee,

J.E., Lindstrom, K.L., Linscott, I.R., Lisse, C.M., Lunsford, A.W., Mallder, V.A., Martin, N., McComas, D.J., McNutt, R.L., Mehoke, D., Mehoke, T., Melin, E.D., Mutchler, M., Nelson, D., Nimmo, F., Nunez, J.I., Ocampo, A., Owen, W.M., Paetzold, M., Page, B., Parker, A.H., Parker, J.W., Pelletier, F., Peterson, J., Pinkine, N., Piquette, M., Porter, S.B., Protopapa, S., Redfern, J., Reitsema, H.J., Reuter, D.C., Roberts, J.H., Robbins, S.J., Rogers, G., Rose, D., Runyon, K.D., Retherford, K.D., Ryschkewitsch, M.G., Schenk, P.M., Schindhelm, E., Sepan, B., Showalter, M.R., Singer, K.N., Soluri, M., Stanbridge, D., Steffl, A.J., Strobel, D.F., Stryk, T., Summers, M.E., Szalay, J.R., Tapley, M., Taylor, A., Taylor, H.W., Throop, H.B., Tsang, C.C.C., Tyler, G.L., Umurhan, O.M., Verbiscer, A.J., Versteeg, M.H., Vincent, M., Webbert, R., Weidner, S., Weigle, G.E., White, O.L., Whittenburg, K., Williams, B.G., Williams, K., Williams, S., Woods, W.W., Zangari, A.M., Zirnstein, E.J., 2015. The Pluto system: Initial results from its exploration by New Horizons. Science (80-.). 350.

Stern, S.A., Kammer, J.A., Barth, E.L., Singer, K.N., Lauer, T.R., Hofgartner, J.D., Weaver, H.A., Ennico, K.A., Olkin, C.B., Young, L.A., 2017. Evidence for Possible Clouds in Pluto's Present-day Atmosphere. Astron. J. 154, 43. https://doi.org/10.3847/1538-3881/aa78ec

Szopa, C., Cernogora, G., Boufendi, L., Correia, J.-J., Coll, P., 2006. PAMPRE: A dusty plasma experiment for Titan's tholins production and study. Planet. Space Sci. 54, 394–404. https://doi.org/https://doi.org/10.1016/j.pss.2005.12.012

Trainer, M.G., Jimenez, J.L., Yung, Y.L., Toon, O.B., Tolbert, M.A., 2012. Nitrogen Incorporation in CH4-N2 Photochemical Aerosol Produced by Far Ultraviolet Irradiation. Astrobiology 12, 315–326. https://doi.org/10.1089/ast.2011.0754

Tziotis, D., Hertkorn, N., Schmitt-Kopplin, P., 2011. Kendrick-Analogous Network Visualisation of Ion Cyclotron Resonance Fourier Transform Mass Spectra: Improved Options for the Assignment of Elemental Compositions and the Classification of Organic Molecular Complexity. Eur. J. Mass Spectrom. 17, 415–421. https://doi.org/10.1255/ejms.1135

Vuitton, V., Bonnet, J.-Y., Frisari, M., Thissen, R., Quirico, E., Dutuit, O., Schmitt, B., Le Roy, L., Fray, N., Cottin, H., Sciamma-O'Brien, E., Carrasco, N., Szopa, C., 2010. Very high resolution mass spectrometry of HCN polymers and tholins. Faraday Discuss. 147, 495–508. https://doi.org/10.1039/C003758C

Wong, M.L., Fan, S., Gao, P., Liang, M.-C., Shia, R.-L., Yung, Y.L., Kammer, J.A., Summers, M.E., Gladstone, G.R., Young, L.A., Olkin, C.B., Ennico, K.A., Weaver, H.A., Stern, S.A., 2017. The photochemistry of Pluto's atmosphere as illuminated by New Horizons. Icarus 287, 110–115. https://doi.org/https://doi.org/10.1016/j.icarus.2016.09.028

Wu, Z., Rodgers, R.P., Marshall, A.G., 2004. Two- and Three-Dimensional van Krevelen Diagrams: A Graphical Analysis Complementary to the Kendrick Mass Plot for Sorting Elemental Compositions of Complex Organic Mixtures Based on Ultrahigh-Resolution

952 Broadband Fourier Transform Ion Cyclotron Resonance. Anal. Chem. 76, 2511–2516.
953 https://doi.org/10.1021/ac0355449

954 Yamashita, M., Fenn, J.B., 1984. Electrospray ion source. Another variation on the free-jet
955 theme. J. Phys. Chem. 88, 4451–4459. https://doi.org/10.1021/j150664a002

956 Young, L.A., Kammer, J.A., Steffl, A.J., Gladstone, G.R., Summers, M.E., Strobel, D.F.,
957 Hinson, D.P., Stern, S.A., Weaver, H.A., Olkin, C.B., Ennico, K.A., McComas, D.J.,
958 Cheng, A.F., Gao, P., Lavvas, P., Linscott, I.R., Wong, M.L., Yung, Y.L., Cunningham,
959 N., Davis, M., Parker, J.W., Schindhelm, E., Siegmund, O.H.W., Stone, J., Retherford,
960 K.D., Versteeg, M.H., 2018. Structure and composition of Pluto's atmosphere from the
961 New Horizons solar ultraviolet occultation. Icarus 300, 174–199.
962 https://doi.org/https://doi.org/10.1016/j.icarus.2017.09.006

963 Young, L.A., Stern, S.A., Weaver, H.A., Bagenal, F., Binzel, R.P., Buratti, B.J., Cheng, A.F.,
964 Cruikshank, D.P., Gladstone, G.R., Grundy, W.M., Hinson, D.P., Horányi, M., Jennings,
965 D.E., Linscott, I.R., McComas, D.J., McKinnon, W.B., McNutt, R.L., Moore, J.M.,
966 Murchie, S., Olkin, C.B., Porco, C.C., Reitsema, H.J., Reuter, D.C., Spencer, J.R., Slater,
967 D.C., Strobel, D.F., Summers, M.E., Tyler, G.L., 2008. New Horizons: Anticipated
968 Scientific Investigations at the Pluto System. Space Sci. Rev. 140, 93–127.
969 https://doi.org/10.1007/s11214-008-9462-9

970 Zhang, X., Strobel, D.F., Imanaka, H., 2017. Haze heats Pluto's atmosphere yet explains its
971 cold temperature. Nature 551, 352.

972 Zhu, X., Strobel, D.F., Erwin, J.T., 2014. The density and thermal structure of Pluto's
973 atmosphere and associated escape processes and rates. Icarus 228, 301–314.
974 https://doi.org/https://doi.org/10.1016/j.icarus.2013.10.011

975